eLife

Reviewed Preprint
v2 • October 3, 2025
Revised by authors

Reviewed Preprint
v1 • April 9, 2025

Neuroscience

Type-I nNOS neurons orchestrate cortical neural activity and vasomotion

Kevin L Turner, Dakota F Brockway, Md Shakhawat Hossain, Keith R Griffith, Denver I Greenawalt, Qingguang Zhang, Kyle W Gheres, Nicole A Crowley, Patrick J Drew

Department of Engineering Science and Mechanics, The Pennsylvania State University, State College, United States • Center for Neural Engineering, The Pennsylvania State University, State College, United States • Department of Biomedical Engineering, The Pennsylvania State University, State College, United States • Penn State Neuroscience Institute, The Pennsylvania State University, State College, United States • Department of Biology, The Pennsylvania State University, State College, United States • Graduate Program in Molecular Cellular and Integrative Biosciences, The Pennsylvania State University, State College, United States • Department of Physiology, Michigan State University, East Lansing, United States • Department of Neurosurgery, The Pennsylvania State University, State College, United States

eLife Assessment

This **important** study provides **solid** evidence for new insights into the role of Type-1 nNOS interneurons in driving neuronal network activity and controlling vascular network dynamics in awake, head-fixed mice. The authors use an original strategy based on the ablation of Type-1 nNOS interneurons with local injection of saporin conjugated to a substance P analogue into the somatosensory cortex. They show that ablation of type I nNOS neurons has surprisingly little effect on neurovascular coupling, although it alters neural activity and vascular dynamics.

https://doi.org/10.7554/eLife.105649.2.sa3

Abstract

It is unknown how the brain orchestrates coordination of global neural and vascular dynamics. We sought to uncover the role of a sparse but unusual population of genetically distinct interneurons known as type-I nNOS neurons, using a novel pharmacological strategic to unilaterally ablate these neurons from the somatosensory cortex of mice. Region-specific ablation produced changes in both neural activity and vascular dynamics, decreased power in the delta-band of the local field potential, reduced sustained vascular responses to prolonged sensory stimulation, and abolished the post-stimulus undershoot in cerebral blood volume. Coherence between the left and right somatosensory cortex gamma-band power envelope and blood volume at ultra-low frequencies was decreased, suggesting type-1 nNOS neurons integrate long-range coordination of brain signals. Lastly, we observed decreases in the amplitude of resting-state blood volume oscillations and decreased vasomotion following the ablation of type-I nNOS neurons. This demonstrates that a small population of nNOS-positive neurons are indispensable for regulating both neural and vascular dynamics in the

whole brain, raising the possibility that loss of these neurons could contribute to the development of neurodegenerative diseases and sleep disturbances.

Introduction

Coordinated neural and hemodynamic activity across the brain are vital for arousal and cognition. The relationship between changes in neural activity and (typically measured) changes in blood volume, flow, and oxygenation, which are frequently studied with hemodynamic imaging and form the foundation of modern neuroscience, are mediated by local vasodilation and is known as neurovascular coupling (Drew 2019, Schaeffer & Iadecola 2021). Neurovascular coupling plays a critical role in supporting neuronal function, as tightly coordinated hemodynamic activity is essential for meeting energy metabolism and maintaining brain health (Iadecola et al 2023, Schaeffer & Iadecola 2021). The vasodilator nitric oxide (NO) (Hosford & Gourine 2019), produced by neuronal nitric oxide synthase (nNOS) in neurons, provides a key mechanism of arteriole dilation. Neurons in somatosensory cortex that express nNOS are activated by sensory stimulation, volitional whisking, and locomotion (Ahn et al 2023, Echagarruga et al 2020), all of which produce robust hemodynamic responses (Huo et al 2014, Winder et al 2017). Chemogenetic elevation or suppression of nNOS neuron activity alters both baseline diameter and behaviorally evoked dilation of arterioles (Echagarruga et al 2020). Similar vascular changes are produced by local infusion of a NOS inhibitor (Echagarruga et al 2020), implicating NO signaling directly in vascular regulation. Optogenetic activation of nNOS-positive neurons produces varying effects, with some reports demonstrating vasodilation and blood flow increases with minimal changes in neural activity (Krawchuk et al 2020, Lee et al 2020, Ruff et al 2024), while others show large, low-frequency EEG changes during sleep and quiet wakeful states (Gerashchenko et al 2018). While NO is known to modulate the excitability of neurons (Kara & Friedlander 1999, Smith & Otis 2003), artificial activation of nNOS neurons seems to drive vascular responses that are disproportionally larger than any corresponding neural changes, suggesting that this small population of neurons has an impact on vascular signals that is substantially greater than that of overall neural activity.

Two distinct GABAergic interneurons types express nNOS, denoted as type-I and type-II (Kawaguchi & Kubota 1997, Kubota et al 2011, Perrenoud et al 2012). nNOS-positive neurons make up approximately 20% of GABAergic interneurons in the cortex (Hendry et al 1987, Sahara et al 2012), with type-I constituting only 0.5–2% depending on brain region (Chong et al 2019, Tricoire & Vitalis 2012, Yan & Garey 1997). Type-I nNOS neurons are sparse, somatostatin-positive, most dense in the deep layers of cortex, and express nNOS at higher levels than type-II. They extend both local and long-range projections throughout the cortex, receive excitatory input from nearby pyramidal neurons and drive increases in cerebral blood flow when stimulated (Ruff et al 2024). Type-II nNOS neurons are in contrast much more abundant, smaller in size and morphology, and express nNOS less strongly than type-I. Type-II are a more heterogeneous group that express a variety of interneuron subtype markers and are more evenly distributed throughout the different layers of cortex (Perrenoud et al 2012, Yan et al 1996). Type-I nNOS neurons have been observed in rodents, carnivores, and primates (Higo et al 2007, Tomioka et al 2005, Tomioka & Rockland 2007) and are active during sleep (Dittrich et al 2015, Gerashchenko et al 2008, Kilduff et al 2011, Morairty et al 2013). In the cortex, type-I nNOS neuron density is anticorrelated with vascular density (Wu et al 2022). Type-I nNOS neurons integrate local activity from feedforward excitatory pathways from the cortex and thalamus, likely contributing to the correlated changes in blood flow that are observed between functionally connected regions across hemispheres (Ruff et al 2024). Molecular, electrophysiological, and immunohistochemistry studies have demonstrated that type-I nNOS neurons are the only cells in the cortex that express the tachykinin receptor 1 (also known as neurokinin 1 receptor, TACR1/NK1R), the primary receptor for the endogenous neuropeptide substance P (Dittrich et al 2012, Endo et al 2016, He et al 2016, Huang et al 2016, Kubota

et al 2011, Matsumura et al 2021, Paul et al 2017, Penny et al 1986, Ruff et al 2024, Vanlandewijck et al 2018, Vruwink et al 2001). Local infusion of substance P into the cortex causes a sustained increase in basal arterial diameter that is dependent upon local neural activity (Echagarruga et al 2020). Type-I nNOS neurons likely receive substance P from the ~40% of parvalbumin (PV)-positive cortical interneurons (Bugeon et al 2022, Pfeffer et al 2013, Vruwink et al 2001) that are thought to drive network synchrony (Cardin et al 2009, Sohal et al 2009). Optogenetic stimulation of PV neurons for several seconds drives a biphasic hemodynamic response, comprised of an early constriction (driven by suppression of overall population activity through GABA release), and a delayed, prolonged dilation lasting tens of seconds that is mediated indirectly by substance P (Vo et al 2023). The delayed vasodilation was not directly related to pyramidal neuron activity, was blocked by TACR1 antagonists, and was occluded by substance P, suggesting that activation of PV neurons drives downstream activation of type-I nNOS neurons. These experiments point to type-I nNOS neurons as having a large effect on vascular dynamics despite their smaller contribution in driving overall neural activity. However, optogenetic stimulation only activates one component of a circuit in isolation, in an otherwise healthy and intact microcircuit, potentially giving an incomplete picture of the neuron's role. Type-I nNOS neurons are uniquely vulnerable to stress (Han et al 2019), and their loss is likely in part causal to neurodegeneration (Iadecola et al 2023, Schaeffer & Iadecola 2021), making it vital to understand brain wide changes following a more physiologically-relevant model of perturbation.

Here we sought to reveal the role of type-I nNOS neurons in controlling neural and vascular dynamics in the cortex by selectively ablating them with saporin conjugated to a substance P analog (SP-saporin). Using this targeted ablation approach, we found that ablation of type-I nNOS neurons caused decreases in the hemodynamic response to sustained vibrissae stimulation, eliminated the post-stimulus undershoot, decreased local field potential power in the delta-band (1-4 Hz), reduced bilateral correlations in gamma-band power and blood volume across arousal states, and reduced the amplitude of resting-state blood volume oscillations. Together, these experiments demonstrate that a small subset of type-I nNOS neurons regulate key neural and vascular dynamics that coordinate changes in vasomotion.

Results

We investigated the effects of localized ablation of type-I nNOS neurons in somatosensory cortex on neurovascular coupling and functional connectivity in unanesthetized, head-fixed mice. C57BL6J mice (119 total, both male and female) were injected with either saporin conjugated to a substance P analog with high affinity for the substance P receptor (SP-SAP) or a scrambled peptide as a control (Blank-SAP) into a localized region of one hemisphere's somatosensory cortex. We used widefield optical imaging, electrophysiology, and 2-photon microscopy to evaluate neural and hemodynamic changes following targeted ablation of type-I nNOS neurons in the vibrissae (whisker) representation of somatosensory cortex while carefully monitoring arousal state (see Materials and Methods). All imaging was performed during the animals' light cycle. Statistics included generalized linear mixed-effects model (GLME), general linear models (GLM), or unpaired t-tests with corrections for multiple comparisons when necessary.

Saporin-conjugated peptides produce selective targeted ablation of type-I nNOS neurons

While optogenetic and chemogenetic models give us insights into the potential function of neuron subtypes, it is difficult to completely silence neurons in vivo, and the patterns of activity they induce are not physiological and can have paradoxical effects on neural activity (Andrei et al 2021, Li et al 2019). Saporin provides a pharmacological route to selectively kill only the cells

that internalize it, and saporin conjugated to a peptide effectively targets neurons that express a receptor for the peptide (Abbott et al 2012, McKay & Feldman 2008), allowing targeting of specific cell types orthogonal to any genetic targeting techniques.

We first sought to validate the efficacy and specificity of saporin-based targeting of cortical TACR1-expressing neurons. Type-I nNOS neurons were ablated by injection of the ribosome inactivating protein saporin (SAP), conjugated either to substance P (SP-SAP) or a scrambled peptide as a control (Blank-SAP) (**Fig. 1a**). The SP-bound SAP toxin binds to TACR1-expressing neurons (Martin & Sloviter 2001, Wang et al 2002, Wiley & Lappi 1999), which in the cortex are exclusively expressed by type-I nNOS neurons (**Fig. 1b**). We used both immunofluorescence (**Fig. 1c**) and NADPH diaphorase staining (a histochemical marker for NOS, **Fig. S1**), to visualize nNOS neuron ablation (Bredt et al 1991, Hope et al 1991, Hope & Vincent 1989). Immunofluorescent labeling in mice injected with Blank-SAP showed labeling of nNOS-positive neurons near the injection site. In contrast, mice injected with SP-SAP showed a clear loss in nNOS-labeling, with a typical spread of 1-2 mm from the injection site, though nNOS-positive neurons both subcortically and in the entirety of the contralateral hemisphere remaining intact. We quantified the efficacy of SP-SAP in removing type-I nNOS neurons by quantifying the number of nNOS-positive neurons per square mm of cortical tissue (**Fig. 1d**), of which SP-SAP injected mice (N = 5, 3M/2F) had a significant reduction of nNOS-labeled neurons (1.3 ± 1.6 neurons/mm^2) compared to Blank-SAP mice (N = 8, 4M/4F) with 10.3 ± 2.4 neurons/mm^2 (GLME $p = 5.74\times10^{-6}$). It is unlikely that the disappearance of type-I nNOS neurons is because they stopped expressing nNOS, as internalized saporin is cytotoxic. Exposure to SP-conjugated saporin causes rapid internalization of the SP receptor-ligand complex (Mantyh et al 1995), and internalized saporin causes cell death via apoptosis (Bergamaschi et al 1996). In the brain, the resulting cellular debris from saporin administration is then cleared by microglia phagocytosis (Seeger et al 1997).

We checked for non-specific effects driven by SP-SAP injections one-month post-administration by staining for ionized calcium binding adaptor molecule 1 (IBA1), glial fibrillary acidic protein (GFAP), DAPI, and NeuN (neuronal nuclei) as well as nNOS (as a positive control for ablation). There was no difference in the number of microglia (**Fig. 1e**) between groups (Blank-SAP: 345.8 ± 47.7 microglia/mm^2; SP-SAP: 373.8 ± 69.4 microglia/mm^2). There was an increase in GFAP labeling following SP-SAP injection (1246.3 ± 514.8 AU/mm^2; Blank-SAP: 527.2 ± 230.9 AU/mm^2, GLME $p = 0.0029$) (**Fig. 1f**). There was no significant difference in DAPI fluorescence (Blank-SAP: 3511.2 ± 524.42 AU/mm^2; SP-SAP: 5180.7 ± 2135.0 AU/mm^2; GLME $p = 0.038$, **Fig. 1g**) or NeuN fluorescence (Blank-SAP: 4296.8 ± 339.4 AU/mm^2; SP-SAP: 4652.1 ± 196.8 AU/mm^2; GLME $p = 0.043$, **Fig. 1h**) between groups after Bonferroni correction for (5) multiple comparisons (**Fig. 1d-h**). Together, these findings indicate that the SP-SAP toxin was highly selective in ablating type-I nNOS neurons with minimal non-specific effects. All mice that underwent imaging were histologically verified for successful type-I nNOS neuron ablation using NADPH diaphorase staining. We quantified a subset of these mice and saw a similar specific removal of type-I nNOS neurons (**Fig. S1**). To determine if ablation of type-I nNOS neurons from the somatosensory cortex had any impact on behavior or arousal state, we assayed exploratory behavior, sleep, and pupil dynamics (**Fig. S2**). To assay exploratory behavior, mice were placed in a novel open field environment and allowed to explore for 5 minutes while quantifying distance traveled and time spent in the center, two metrics for evaluating stress and anxiety in rodents (Roth & Katz 1979, Seibenhener & Wooten 2015). We noted no differences in any metric evaluating open field behavior (N = 12-23 mice/group). We also assessed multiple measurements of sleep quality and quantity. There was no difference in the percentage of time each mouse spent in rapid eye movement (REM) or non-REM (NREM) sleep, or the percentage of time they spent volitionally whisking while awake (N = 9 mice/group). We also noted no significant differences in eye-related arousal state metrics including interblink-interval, pupil size, and pupillary response to vibrissae stimulation (Turner et al 2023). Together, this suggests that ablation of type-I nNOS neurons had no gross effects on sleep or general ambulatory behavior.

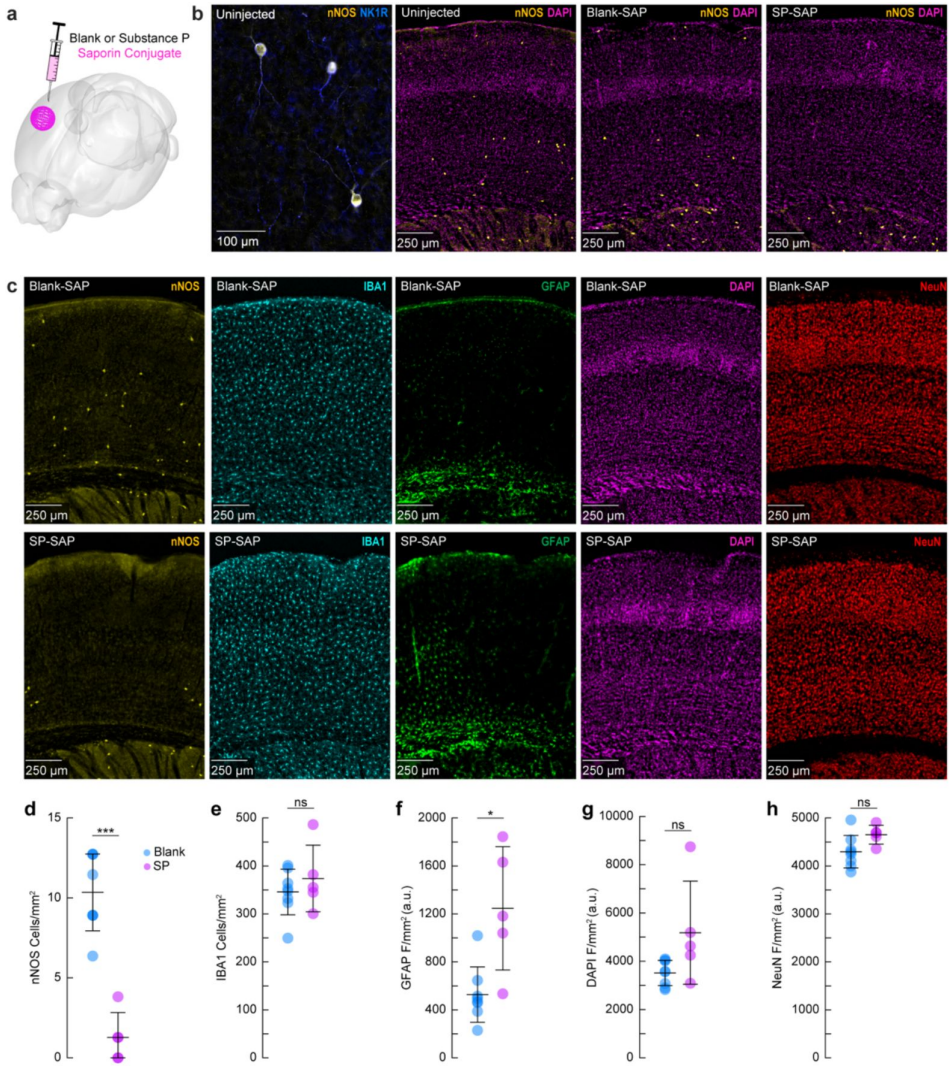

Figure 1.

Saporin-conjugated peptides produce selective targeted ablation of type-I nNOS neurons

(a) Schematic showing intracortical administration of the ribosome inactivating protein saporin conjugated to either SP or a vehicle control. **(b)** Representative immunofluorescence of anti-nNOS (yellow) and anti-NKR1 (blue) showing colocalization of the NK1 receptor on cortical nNOS-positive neurons. Representative immunofluorescence of anti-nNOS (yellow) and DAPI (magenta) from animals with no injection (Uninjected, left), Blank-SAP (middle), or SP-SAP (right). **(c)** Representative immunofluorescence of Blank-SAP (top) and SP-SAP (bottom) sections co-stained with nNOS (left), IBA1 (middle left), GFAP (middle), DAPI (middle right), or NeuN (right). NeuN image was taken from section immediately adjacent to the first four. **(d)** Quantification of nNOS counts, **(e)** IBA1 counts, **(f)** GFAP fluorescence, **(g)** DAPI fluorescence, **(h)** NeuN fluorescence. Error bars **(d-h)** denote SD. Bonferroni correction (5) *α < 0.01, **α < 0.002, ***α < 0.002. **k-l** *α < 0.05, **α < 0.01, ***α < 0.001, GLME.

Impact of type-I nNOS neuron removal on neural and hemodynamic signals across arousal states

To determine the impact localized ablation of type-I nNOS neurons had on neural and hemodynamic signals in the somatosensory cortex, we used widefield optical imaging (Huo et al 2014, Sirotin & Das 2009) to measure changes in total hemoglobin (Δ[HbT], an indicator of blood volume). We measured neural activity using either implanted electrodes (Winder et al 2017) to measure changes in local field potential (LFP) (**Fig. 2a, c, d**), or in a separate cohort of mice, pan-neuronal expression of the calcium indicator GCaMP7s (Chan et al 2017, Dana et al 2019), which provides complementary measures of bulk neural activity (**Fig. 2b, e, f**). In mice expressing GCaMP7s, we measured Δ[HbT], as well as changes in cerebral oxygenation (Δ[HbO]) and deoxygenation (Δ[HbR]) using alternating illumination at 480/530/630 nm (Ma et al 2016a, Ma et al 2016b, Zhang et al 2019). We corrected for hemodynamic contamination of GCaMP7s signals using the simultaneously acquired hemoglobin signals (Kramer & Pearlstein 1979, Ma et al 2016a, Scott et al 2018, Wright et al 2017). Measurements of neural and hemodynamic signals were taken bilaterally through polished and reinforced thinned-skull windows (Drew et al 2010, Shih et al 2012) in the vibrissae representation of somatosensory cortex. Each animal was habituated to head-fixation over the course of several days following surgery. For the first 60 minutes of each recording session, the vibrissae were briefly stimulated with directed puffs of air to either the left or right pad, or by a puffer directed away from the mouse as an auditory control (Drew et al 2011). Afterwards, each mouse was given several hours to naturally sleep with no stimulation. To determine the arousal state of the mouse, we performed electromyography of the nuchal muscles of the neck, tracked vibrissae movement and pupil diameter using video, and body movements with a force sensor. Arousal state was scored in 5 second intervals as either Awake, NREM, or REM as previously described (Turner et al 2020) from behavioral and physiological data using a bootstrapped random forest classification algorithm. We saw no differences in the accuracy or validity of our sleep-scoring models across different experimental conditions (Blank-SAP; SP-SAP; Uninjected) (**Fig. S3**).

Ablation of type-I nNOS neurons reduces the stimulus-evoked response

We first determined the impact of removal of type-I nNOS neurons on evoked hemodynamic signals. The initial increase in blood volume in response to brief (0.1 second) stimulation of the contralateral vibrissae was not affected by ablation of type-I nNOS neurons (**Fig. 3a**), but the post-stimulus undershoot was absent in the SP-SAP mice. When we evaluated the canonical post-stimulus hemodynamic undershoot from 2:4 seconds, the Blank-SAP group (N = 9, 5M/4F) had a mean of −2.2 ± 0.5 μM, compared to the SP-SAP group (N = 9, 5M/4F) mean of 1.0 ± 0.6 μM (GLME p = 0.0005). This result is consistent with the observation that type-I nNOS neurons express the vasoconstrictory neuropeptide Y (NPY) (Karagiannis et al 2009) which is thought to underlie this post-stimulus undershoot (Uhlirova et al 2016). It is also possible that loss of NO signaling from type-I nNOS neurons could also contribute through interactions with blood volume to generate oscillations and post-dilation undershoots (Haselden et al 2020). Using three-wavelength spectroscopy in mice expressing GCaMP7s, we saw consistent increases in blood volume, neural activity, and cerebral oxygenation during prolonged (5 seconds) vibrissae stimulation. Δ[HbT] evaluated 1.5:6.5 seconds following stimulus-onset decreased from 18.7 ± 1.7 μM in Blank-SAP (N = 7, 3M/4F) to 13.1 ± 1.4 μM in SP-SAP (N = 8, 4M/4F, GLME p = 0.017) (**Fig. 3b**). Calcium signals (**Fig. 3c**) evaluated 2:5 seconds following stimulus onset decreased from 8.2 ± 1.3 % in Blank-SAP to 5.3 ± 0.7 % in SP-SAP (GLME p = 0.047). Δ[HbO] (**Fig. 3d**) evaluated 1.5:6.5 seconds following stimulus onset decreased from 24.6 ± 1.9 μM in Blank-SAP to 17.4 ± 1.7 μM in SP-SAP (GLME p =

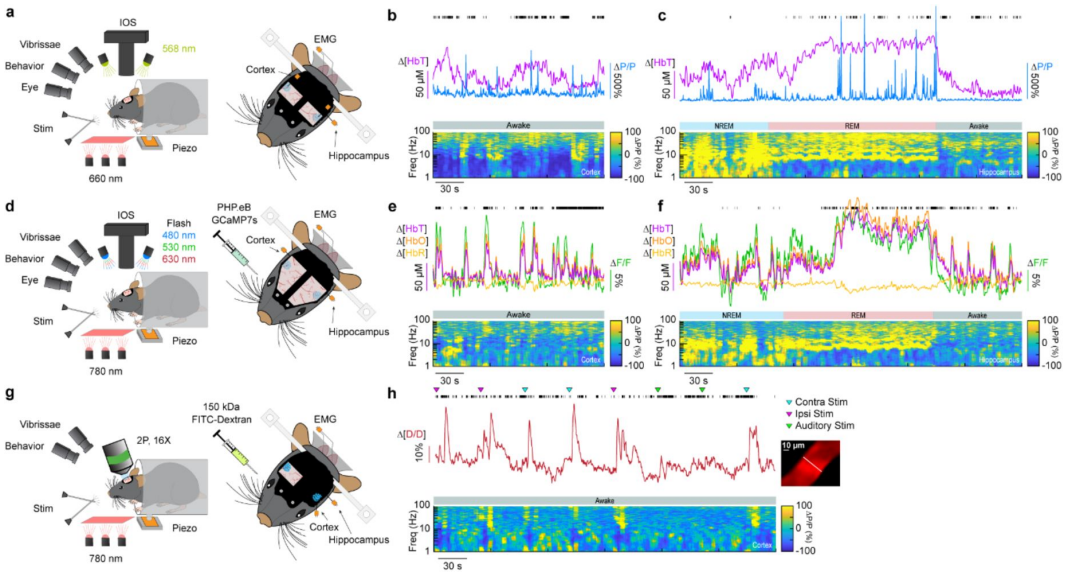

Figure 2.

Impact of type-I nNOS neuron removal on neural and hemodynamic signals across arousal states

(a) Schematic of widefield optical imaging experimental setup. The brain is illuminated at an isosbestic wavelength of hemoglobin (568 nm). Changes in reflected light measuring changes in total blood volume are captured by a camera mounted above the head while several other cameras monitor animal behavior and arousal state including vibrissae and pupil tracking. Vibrissae stimulation is done by directed air puffs. Polished and reinforced thinned-skull windows were bilaterally implanted over the somatosensory cortex. Tungsten stereotrodes were implanted underneath each window to record changes in local field potential within the area of interest (relative change in power, ΔP/P). An additional hippocampal stereotrode and a neck electromyography electrode were used to assist in sleep scoring. **(b,e,h)** During the awake state, power in low-frequency cortical LFP is low and power in the gamma-band (30-100 Hz) is elevated during activity such as volitional whisking. **(c, f)** Periods of NREM and REM sleep are accompanied by large oscillations in cerebral blood volume, with large increases in power in delta-band (1-4 Hz) cortical LFP during NREM and large increases in theta-band (4-10 Hz) hippocampal LFP during REM. Black tick marks indicate vibrissae motion. **(d)** Schematic of widefield optical imaging experiments with GCaMP7s. Alternating illumination with 480 nm, 530 nm, and 630 nm light were used to measure changes in total hemoglobin, blood oxygenation, and GCaMP7s fluorescence. (g) Schematic of two photon experiments.

0.010) while Δ[HbR] evaluated from 1.5:6.5 seconds increased from −6.0 ± 0.4 in Blank-SAP to −4.4 ± 0.3 in SP-SAP (GLME p = 0.005). Evaluation windows were determined based on the duration of stimuli and the delayed onset of the hemodynamic response.

We further investigated single arterial dynamics during vibrissae stimulation with 2-photon microscopy. Following ablation of type-I nNOS neurons, after vibrissae stimulation there was a decrease in arteriole diameter (**Fig. 3e**) evaluated 3:7 seconds following stimulus onset from 11.6 ± 0.8 %·s in Blank-SAP (N = 9, 5M/4F, n = 81 arterioles) down to 7.8 ± 0.6 % in SP-SAP (N = 7, 2M/5F, n = 70 arterioles, GLME p = 0.008). The arterial changes closely mirror the Δ[HbT] changes, consistent with the substantial contribution of arterial dynamics to the blood volume signal (Huo et al 2015). We also evaluated changes in blood volume during voluntary locomotion, where we saw a similar trend in decrease in locomotion-evoked Δ[HbT] evaluated 1.5:2.5 seconds following locomotion onset from 17.5 ± 2.0 μM in Blank-SAP (N = 7, 5M/2F) to 12.9 ± 2.0 μM in SP-SAP (N = 7, 2M/5F), but it was not statistically significant (GLME p = 0.10). These results show the removal of a very small number of neurons can drive substantial reductions in both hemodynamic and neural response to sensory stimulation.

Type-I nNOS ablation reduces low frequency neural activity and gamma-band neurovascular coupling

To determine the effect that type-I nNOS neuron removal had on neural activity, we assessed the power spectrum of the LFP in different arousal states, which we classified into alert, asleep, and all data (Turner et al 2020). Data was classified into the alert state when 15-minute blocks were predominantly (> 80%) in the awake state. Alert periods contained fidgeting movements and bouts of whisking interspersed with awake quiescence. Periods classified as asleep were predominantly composed of sleeping states (NREM/REM > 80% of all classifications in a 15-minute block) with only brief periods of wakefulness, typically occurring during transitions between sleep states. The 'all' state includes everything irrespective of arousal state classification. The first ~60 minutes of each recording session which included vibrissae stimulation was excluded. There was a pronounced reduction in the delta-band (1-4 Hz) power of the LFP in all three arousal state categories. The power in the delta-band of the LFP in Blank-SAP mice (N = 9, 4M/5F) in the alert state (**Fig. 4a**) was $3.4\times10^{-10} \pm 1.0\times10^{-10}$ a.u. compared to $1.0\times10^{-10} \pm 3.0\times10^{-11}$ a.u. in the SP-SAP mice (N = 9, 5M/4F, GLME p = 0.011). The power in the delta-band of the LFP in Blank-SAP mice (N = 7, 3M/4F) in the asleep state (**Fig. 4b**) was (NREM + REM) was $8.5\times10^{-10} \pm 3.0\times10^{-10}$ a.u. compared to $2.4\times10^{-10} \pm 9.1\times10^{-11}$ a.u. in the SP-SAP mice (N = 7, 4M/3F, GLME p = 0.022). The power in the delta-band of the LFP in Blank-SAP mice (N = 9, 4M/5F) averaged across all arousal states (**Fig. 4c**) was $5.2\times10^{-10} \pm 1.7\times10^{-10}$ a.u. compared to $1.5\times10^{-10} \pm 4.3\times10^{-11}$ a. u. in the SP-SAP mice (N = 9, 5M/4F, GLME p = 0.016). These result parallel those seen in studies where knockout of nNOS produces lower delta band power (Morairty et al 2013) and optogenetic stimulation of nNOS neurons produces low frequency oscillations (Zielinski et al 2019), suggesting that type-I nNOS neurons promote these slow oscillations via NO release. In contrast to the observed reductions in LFP in the ablated hemisphere, we noted no gross changes in the power spectra of neural LFP in the unablated hemisphere (**Fig. S7**) or power of the cerebral blood volume fluctuations in either hemisphere (**Fig. S4**).

We next wanted to see whether the amount of neural activity and corresponding Δ[HbT] in response to vibrissae stimulation was altered following type-I nNOS neuron ablation. As a measure of neurovascular coupling, we used the slope of the line fitting the change in gamma-band power vs. Δ[HbT] following brief (0.1 second) vibrissae stimulation (**Fig. 4d**). Decreases in the slope indicate a smaller vascular response for a given amount of neural activity, indicating a decrease in neurovascular coupling. We found the slope was significantly increased in SP-SAP mice compared to Blank-SAP mice (Blank-SAP: 0.02 ± 0.03; SP: 0.005 ± 0.006, GLM p = 0.0001). We also evaluated the change in GCaMP7s fluorescence vs. Δ[HbT] during prolonged (5 seconds) vibrissae stimulation from 2:5 seconds (**Fig. 4e**) and saw no significant change in the slope

Figure 3.

Ablation of type-I nNOS neurons reduces the stimulus-evoked response

(a) Change in total hemoglobin in response to brief (0.1 second) vibrissae stimulation. **(b)** Change in total hemoglobin in response to extended (5 seconds) vibrissae stimulation. **(c)** Change in GCaMP fluorescence in response to extended vibrissae stimulation. **(d)** Change in oxy- and deoxy-hemoglobin in response to extended vibrissae stimulation. **(e)** Change in arteriole diameter in response to extended vibrissae stimulation. Error bars represent population averages ± SEM. All statistics were evaluated between the indicated intervals. *p < 0.05, **p < 0.01, ***p < 0.001, GLME.

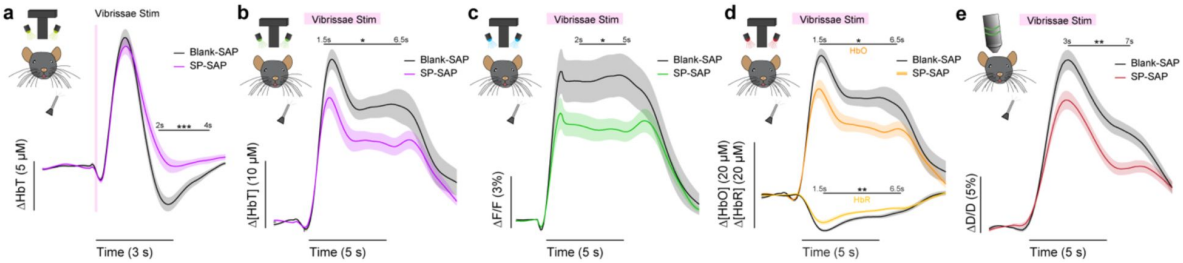

Figure 4.

Type-I nNOS ablation alters low frequency neural activity and gamma-band neurovascular coupling

(a) Local field potential within the vibrissae representation of somatosensory cortex during periods of Alert. **(b)** Asleep. **(c)** All data. **(d)** Change in gamma-band power vs. Δ[HbT] following brief (0.1 seconds) vibrissae stimulation. **(e)** Change in GCaMP7s fluorescence vs. Δ[HbT] following prolonged (5 seconds) vibrissae stimulation. Error bars represent population averages ± SEM. All statistics were evaluated between the indicated intervals. *p < 0.05, **p < 0.01, ***p < 0.001, GLME (**a-c**), GLM (**d, e**).

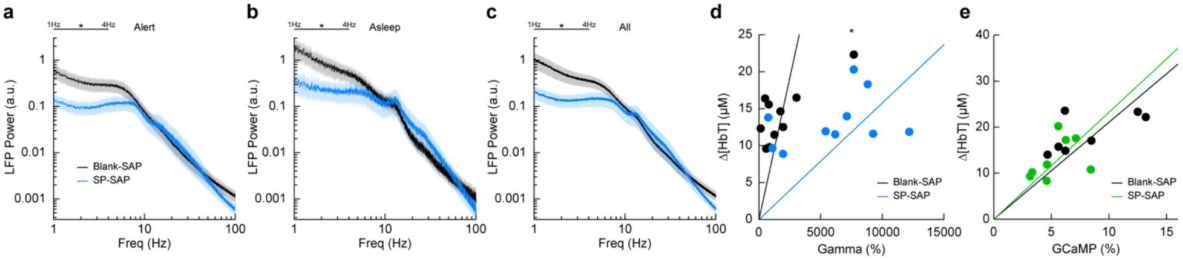

(Blank-SAP: 251.3 ± 75.3; SP: 256.5 ± 73.2, GLM p = 0.34). Given that the sensory-evoked LFP is driven more by synaptic input, while GCaMP7s signals are driven by local neural activity, these results indicate that the loss of type-I nNOS neurons reduces overall excitability, but that the input drive from other areas might be increased, potentially due to homeostatic mechanisms at the input synapses (Turrigiano 2008).

Neurovascular coupling was weakly affected by type-I nNOS removal

We next looked at the cross-correlation between blood volume and neural signals, which provides a measure of spontaneous neurovascular coupling. For electrophysiological measures, we measured the cross-correlation between gamma-band power and blood volume (**Fig. 5a**). We evaluated the peak cross-correlation during the resting-state, during long periods while alert, or long periods while asleep. The cross-correlation between neural activity and hemodynamic signals is substantially higher during periods of behavior (whisking, fidgeting) than during the resting-state because self-generated motion and whisking drive increases in neural activity and vasodilation (Claron et al 2023, Drew et al 2019, Stringer et al 2019, Tu et al 2024, Winder et al 2017) . The correlation between neural activity and blood volume changes is higher during sleep than in the awake state (Turner et al 2020). We saw no significant difference in the peak cross-correlation during the resting-state (**Fig. 5b**) between Blank-SAP mice (N = 9, 4M/5F, 0.08 ± 0.007) and SP-SAP mice (N = 9, 5M/4F, 0.06 ± 0.008, GLME p = 0.22). We did observe a significant difference in the peak cross-correlation during both periods of alert and asleep, from 0.23 ± 0.01 (Blank-SAP) to 0.16 ± 0.03 (SP-SAP, GLME p = 0.036) during alert periods (**Fig. 5c**) and 0.40 ± 0.02 (Blank-SAP) dropping to 0.33 ± 0.02 (SP-SAP, GLME p = 0.012) while asleep (**Fig. 5d**). We next wanted to evaluate whether this drop in neurovascular coupling was more prevalent at a particular modulation frequency. When analyzing the coherence between the gamma-band power and hemodynamic signals during these different arousal states, we noted no dominant frequency and saw no significant changes in the lower frequencies associated with neurovascular coupling (≤ 0.5 Hz). During the resting-state (**Fig. 5e**), the average coherence between 0.1 and 0.5 Hz was 0.28 ± 0.008 in Blank-SAP mice and 0.23 ± 0.01 in SP-SAP mice (GLME p = 0.23). The average coherence between 0.01 and 0.5 Hz during alert periods (**Fig. 5f**) was 0.29 ± 0.004 in Blank-SAP mice and 0.25 ± 0.005 in SP-SAP mice (GLME p = 0.06), and during asleep periods (**Fig. 5g**) it was 0.34 ± 0.008 in Blank-SAP mice and 0.32 ± 0.007 in SP-SAP mice (GLME p = 0.46). Lastly, to evaluate any changes in the predictive power of the neural-hemodynamic relationship, we fit a hemodynamic response function using the gamma-band power and hemodynamic response following periods of vibrissae stimulation. We observed that ablation of Type-I nNOS neurons did not alter the predictive power of the hemodynamic response function (**Fig. S5**).

We next evaluated neurovascular coupling from optical measures of bulk activity using GCaMP7s (**Fig. 5h**). The peak resting-state cross-correlation (**Fig. 5i**) between GCaMP7s fluorescence and ongoing hemodynamics showed a significant decrease, 0.68 ± 0.02 with Blank-SAP versus 0.62 ± 0.02 with SP-SAP (GLME p = 0.038). However, there was no drop in peak cross-correlation during either alert or asleep as seen with the gamma-band power. During alert periods (**Fig. 5j**), the peak GCaMP7s cross-correlation was 0.78 ± 0.12 with Blank-SAP and 0.77 ± 0.02 with SP-SAP (GLME p = 0.54) while during asleep periods (**Fig. 5k**) it was 0.88 ± 0.008 with Blank-SAP and 0.86 ± 0.04 with SP-SAP (GLME p = 0.58). Like the peak in cross-correlation, the average resting-state coherence (**Fig. 5l**) did show a significant drop across the lower frequencies, 0.75 ± 0.01 with Blank-SAP vs. 0.70 ± 0.01 with SP-SAP (GLME p = 0.049). There was no drop in coherence during alert periods (**Fig. 5m**) at 0.78 ± 0.005 with Blank-SAP and 0.77 ± 0.004 with SP-SAP (GLME p = 0.42) nor during asleep periods (**Fig. 5n**) at 0.75 ± 0.009 with Blank-SAP and 0.74 ± 0.01 with SP-SAP (GLME p = 0.63). While there are small changes in neural-hemodynamic correlations, the differences in neurovascular coupling across arousal states were relatively small following localized removal of type-I nNOS neurons, meaning any effects of ablation on hemodynamic responses are primarily mediated by changes in neural activity.

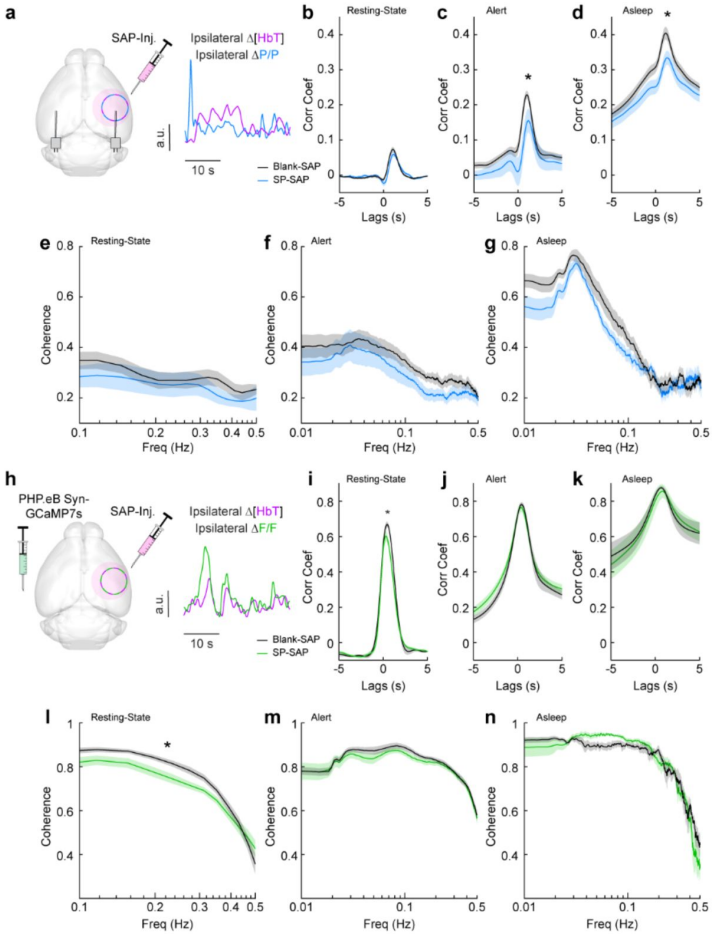

Figure 5.

Neurovascular coupling was only weakly affected by type-I nNOS removal

(a) Schematic demonstrating intracortical injection of either Blank-SAP or SP-SAP and the analysis of gamma-band power and hemodynamic signals from within the vibrissae representation of somatosensory cortex, N = 9 mice per group. **(b)** Gamma-Δ[HbT] resting-state cross-correlation **(c)** Gamma-Δ[HbT] alert cross-correlation **(d)** Gamma-Δ[HbT] asleep cross-correlation **(e)** Gamma-Δ[HbT] resting-state coherence **(f)** Gamma-Δ[HbT] alert coherence **(g)** Gamma-Δ[HbT] asleep coherence **(h)** Schematic demonstrating intracortical injection of either Blank-SAP or SP-SAP and the analysis of GCaMP7s fluorescence and hemodynamic signals from within the vibrissae cortex, n = 6-7 mice per group. **(i)** GCaMP7s-Δ[HbT] resting-state cross-correlation **(j)** GCaMP7s-Δ[HbT] alert cross-correlation (k) GCaMP7s-Δ[HbT] asleep cross-correlation **(l)** GCaMP7s-Δ[HbT] resting-state coherence **(m)** GCaMP7s-Δ[HbT] alert cross-correlation **(n)** GCaMP7s-Δ[HbT] asleep cross-correlation. Error bars represent population averages ± SEM. *p < 0.05, **p < 0.01, ***p < 0.001, GLME.

Type-I nNOS ablation reduces low-frequency interhemispheric coherence

Because type-I nNOS neurons send and receive many modulatory signals across a range of distances, they could help serve to coordinate neural and vascular dynamics across the brain. We tested this hypothesis by comparing how loss of type-I nNOS neurons changed the coherences of neural and hemodynamics signals between the left and right vibrissae cortex, which are generally highly correlated across all behaviors and frequencies (Turner et al 2020). Neural activity is also bilaterally correlated, though less so than vascular dynamics. Average resting-state coherence between the left and right Δ[HbT] signals (**Fig. 6a**) in the vibrissae cortex were 0.79 ± 0.005 for Blank-SAP and 0.73 ± 0.008 for SP-SAP mice (p = 0.014, GLME, **Fig. 6b**). This reduction in coherence was seen over all frequencies (0-0.5 Hz) during both alert periods (**Fig. 6c**), at 0.86 ± 0.002 for Blank-SAP and 0.81 ± 0.003 for SP-SAP ($p = 7.4\times10^{-6}$, GLME), as well as asleep periods (**Fig. 6d**) with 0.86 ± 0.003 for Blank-SAP and 0.79 ± 0.005 for SP-SAP (p = 0.0008, GLME).

We then looked at the coherence of gamma-band power across hemispheres, where average coherence for bilateral gamma-band signals in the resting-state were 0.19 ± 0.006 (Blank-SAP) and 0.19 ± 0.01 (SP-SAP, p = 0.88, GLME, **Fig 6e, f**). There was no significant difference during the alert periods (**Fig 6g**) at 0.22 ± 0.005 (Blank-SAP) and 0.20 ± 0.006 (SP-SAP, p = 0.43, GLME), but ablation of type-I nNOS neuros produced a reduction of coherence during asleep periods (**Fig. 6h**) at 0.35 ± 0.009 (Blank-SAP) and 0.29 ± 0.009 (SP-SAP, p = 0.047, GLME).

Average resting-state coherence across bilateral Δ[HbT] signals (**Fig. 6i**) taken from the vibrissae cortex were 0.83 ± 0.005 (Blank-SAP) and 0.78 ± 0.007 (SP-SAP, p = 0.021, GLME, **Fig. 6j**). This reduction in coherence persisted across all frequencies during the both alert periods (**Fig. 6k**) at 0.92 ± 0.001 (Blank-SAP) and 0.90 ± 0.001 (SP-SAP, p = 0.012, GLME) as well as sleep periods (**Fig. 6l**) at 0.90 ± 0.002 (Blank-SAP) and 0.83 ± 0.005 (SP-SAP, p = 0.004, GLME). Average resting-state coherence across bilateral GCaMP7s signals (**Fig. 6m**) taken from the vibrissae cortex were 0.75 ± 0.009 (Blank-SAP) and 0.70 ± 0.009 (SP-SAP, GLME p = 0.12, **Fig. 6n**). This reduction in coherence persisted across all frequencies during the both alert periods (**Fig. 6o**) at 0.88 ± 0.003 (Blank-SAP) and 0.84 ± 0.003 (SP-SAP, p = 0.029, GLME) but not in sleep periods (**Fig. 6p**) at 0.85 ± 0.005 (Blank-SAP) and 0.84 ± 0.005 (SP-SAP, GLME p = 0.52). When the correlation of bilateral signals was evaluated with Pearson's correlation coefficients, the same general trend remained (**Fig. S6**). These results show that removal of type-I nNOS neurons reduces both vascular and neural coordination across hemispheres. This loss of coherence does not imply that removal of type-I nNOS neurons has direct effects on the contralateral hemisphere, just that the dynamics in the ablated hemisphere have been altered so they no longer respond effectively to input from the ipsilateral hemisphere and/or common sources of modulatory drive that act through type 1 nNOS neurons (e.g. hypocretin (Williams et al 2019), or cholinergic inputs (Williams et al 2018)).

Type-I nNOS neurons control vasomotion power but not baseline diameter

We next wanted to establish how ablation of type-I nNOS neurons affected vasomotion, spontaneous oscillations in the absence of behavior, measured at the scale of blood volume and at the level of single arterioles, as well as the basal tone of blood vessels. The variance in Δ[HbT] during rest, a measure of vasomotion amplitude, was significantly reduced following type-I nNOS ablation (**Fig. 7a**), dropping from 40.9 ± 3.4 μM^2 in the Blank-SAP group (N = 24, 12M/12F) to 23.3 ± 2.3 μM^2 in the SP-SAP group (N = 24, 11M/13F) (GLME $p = 6.9\times10^{-5}$) with no significant difference in the unablated hemisphere (Fig. S7). Individual pial and penetrating arterioles showed the same reduction in vasomotion after type-I nNOS neuron ablation, with Blank-SAP (N = 9, 5M/4F, n = 70 arterioles) having a resting diameter variance of 12.6 ± 1.4 $\%^2$ and SP-SAP (N = 7, 2M/5F, n = 65

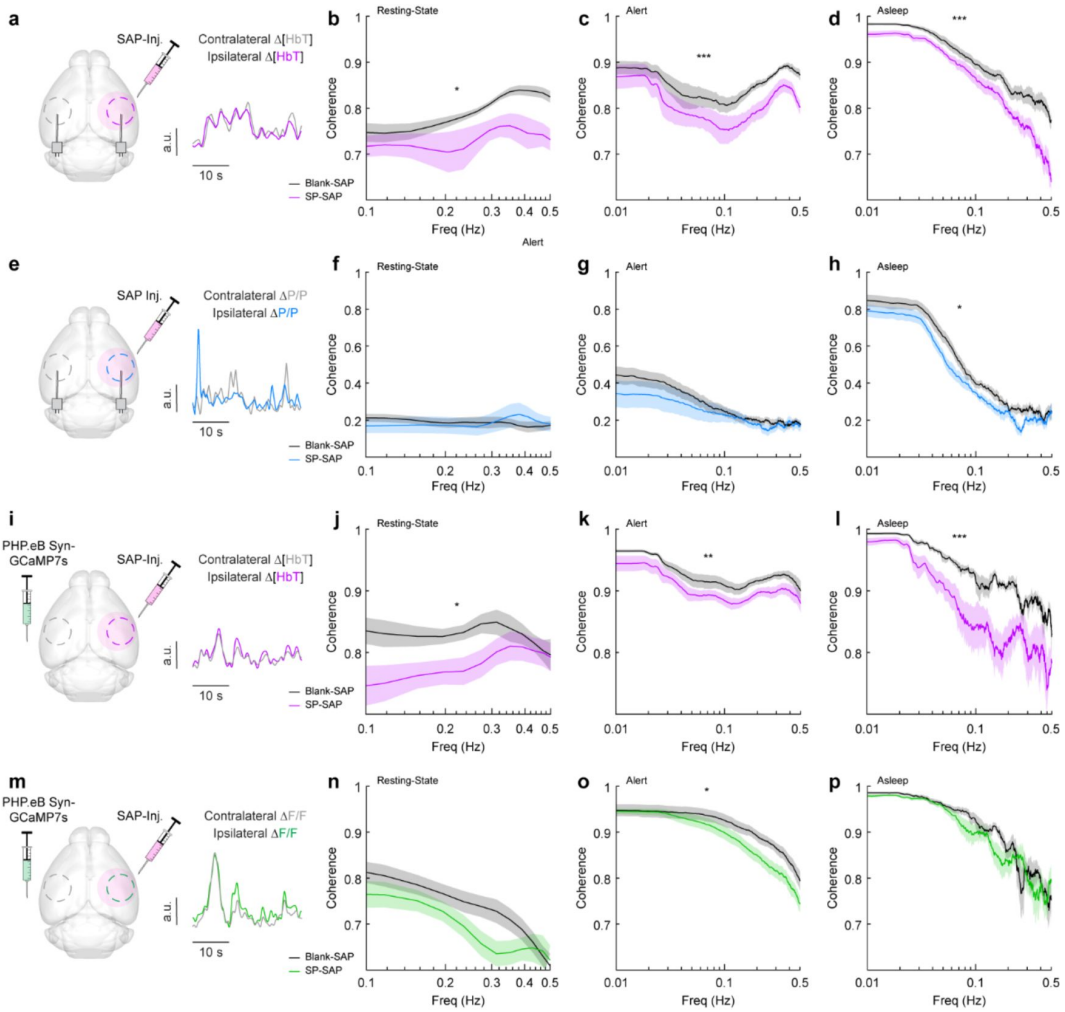

Figure 6.

Type-I nNOS ablation reduces low-frequency interhemispheric coherence

(a) Δ[HbT] coherence between bilateral ROIs in the left and right hemisphere's somatosensory cortex during **(b)** Res.t **(c)** Alert. **(d)** Asleep. **(e)** Gamma-band power coherence between bilateral ROIs in the left and right hemisphere's somatosensory cortex during **(f)** Res.t **(g)** Alert. **(h)** Asleep. **(i)** Δ[HbT] coherence between bilateral ROIs in the left and right hemisphere's somatosensory cortex during **(j)** Res.t **(k)** Alert. **(l)** Asleep. **(m)** GCaMP7s coherence between bilateral ROIs in the left and right hemisphere's somatosensory cortex during **(n)** Res.t **(o)** Alert. **(p)** Asleep. Error bars represent population averages ± SEM. *p < 0.05, **p < 0.01, ***p < 0.001, GLME.

arterioles) of 8.0 ± 0.8 %^{2} (**Fig. 7b**). There was no difference in resting-state (baseline) diameter between the groups, with Blank-SAP having a diameter of 24.4 ± 7.5 μm and SP-SAP having a diameter of 23.0 ± 9.4 μm (ttest, p = 0.61).

If type-I nNOS neurons control the basal diameter of vessels via secreted vasodilators, potentially in an arousal state dependent way, when we ablate these neurons we would observe a difference in blood volume across arousal states and in the maximal dilation elicited with isoflurane (Gao et al 2015). We saw no changes in the average change in Δ[HbT] across states (**Fig. 7c**, **Fig. S8**). The resting-state Δ[HbT] in Blank-SAP mice was 0.29 ± 0.7 μM compared to 0.29 ± 0.9 μM in SP-SAP (GLME p = 0.997). NREM Δ[HbT] in Blank-SAP mice was 23.9 ± 5.8 μM compared to 24.1 ± 6.5 μM in SP-SAP (GLME p = 0.96). REM Δ[HbT] in Blank-SAP mice was 74.5 ± 8.4 μM compared to 82.3 ± 17 μM in SP-SAP (GLME p = 0.26). The Δ[HbT] following isoflurane in Blank-SAP mice was 170.9 ± 19.7 μM compared to 190.5 ± 30.5 μM in SP-SAP (GLME p = 0.15). We repeated the isoflurane experiment on a set of pial and penetrating arterioles under 2-photon microscopy. The change in normalized arteriole diameter following administration of isoflurane (n = 7-9 mice per group, 18-19 arterioles per group) was 61.2 ± 37.2% in Blank-SAP (baseline diameter 23.2 ± 6.6 μm) compared with 63.6 ± 38.4% in SP-SAP (baseline diameter 23.0 ± 10.2 μm, p = 0.85, ttest). These results indicate that type-I nNOS neurons play a role in driving spontaneous hemodynamic fluctuations, but not in setting the basal diameter during different states.

Discussion

We selectively ablated type-I nNOS neurons from the somatosensory cortex, which had marked effects on neural activity and vascular dynamics, but minimal changes in neurovascular coupling. These results are surprising given previous work showing stimulation of these neurons in isolation causes vasodilation and minimal neural activity changes. Our approach of using SP-conjugated saporin allowed a nongenetic means of targeting a critical neuronal cell type, supporting further exploration of the role of type-I nNOS neurons in transgenic mouse models of disease without complicated breeding schemes, as well as in non-model organisms. Our results point to these neurons being an important orchestrator of neural and vascular dynamics, as loss of these neurons causes desynchronization between hemispheres of both neural and vascular signals, as well as altered responses to sensory stimulation. While previous studies using specific activation of type-I nNOS neurons have emphasized the roles of these neurons in driving vasodilation with minimal changes in neural activity, our results point to a larger role of these neurons in organizing and patterning both spontaneous and sensory-evoked neural activity. This is likely due to a loss in NO signaling as well as a loss of the many of the other neuropeptides expressed by type-I nNOS neurons, which all have known effects on other neurons. Loss of type-I nNOS neurons drove minimal changes in the vasodilation elicited by brief stimulation, but led to decreased vascular responses to sustained stimulation, suggesting that the early phase of neurovascular coupling is not mediated by these cells, consistent with the multiple known mechanisms for neurovascular coupling (Attwell et al 2010, Drew 2019, Hosford & Gourine 2019) acting through both neurons and astrocytes with multiple timescales (Le Gac et al 2025, Renden et al 2024, Schulz et al 2012, Tran et al 2018).

While previous studies have found that activation of type-I nNOS neurons, either optogenetically or via administration of substance P, results in vasodilation (which would imply an important role for these neurons for neurovascular coupling), our work provides insight into the integrated function of type-I nNOS neurons in neural circuits and vascular dynamics. Importantly, methodological approaches differentiate our strategy from previous published work. A limitation of our study is the necessary delay between targeted ablation and in vivo imaging for the animals to recover from surgical procedures. With imaging beginning four weeks after ablation, there could be compensatory rewiring of local and/or network activity following type-I nNOS ablation, where other signaling pathways from the neurons to the vasculature become strengthened to

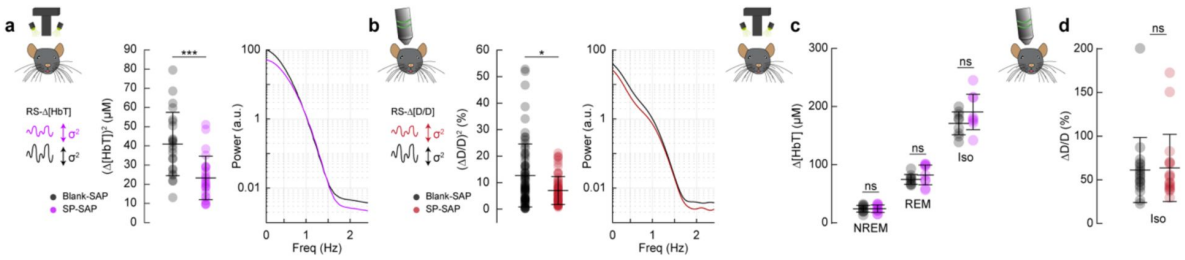

Figure 7.

Type-I nNOS neurons control vasomotion power but not baseline diameter

(a) Variance (proportional to average power) in the resting-state hemodynamics signals measured with widefield optical imaging. **(b)** Variance in resting-state arteriole diameter measured with two-photon. **(c)** Average Δ[HbT] during periods of NREM sleep, periods of REM sleep, and following administration of isoflurane (n = 9 mice per group). **(d)** Change in normalized arteriole diameter following administration of isoflurane. Error bars represent population averages ± SD. All statistics were evaluated between the indicated intervals. *p < 0.05, **p < 0.01, ***p < 0.001 GLME.

compensate for the loss of vasodilatory signaling from the type-I nNOS neurons. While this likely happens to some degree, this interpretation is less likely to completely account for the effect given these potential compensatory changes do not prevent large changes in neural activity and resting vasomotion. Second, there may be some non-linear interactions between vasodilatory signals and/or the vasodilator mechanisms that are arousal-state-dependent. Intrinsic optical signal readout is primarily weighted toward superficial tissue given the absorption and scattering characteristics of the wavelengths used. While surface vessels are tightly coupled with neural activity, it is still a matter of debate whether surface or intracortical vessels are a more reliable indicator of ongoing activity (Goense et al 2012, Huber et al 2015, Poplawsky & Kim 2014). The diameter of arteries tracks the smooth muscle membrane potential linearly, up until a saturation point above which any hyperpolarization does not induce further dilation (Hill 2012, Knot & Nelson 1998, Wölfle et al 2011). Many vasoactive pathways from neurons to vessels are known to exist, whose individual effects added together sum to larger than observed changes in vasodilation (Hosford & Gourine 2019), suggesting a non-linear interaction. It may be that for dilation occurring during sensory stimulation and sleep, the vasodilatory stimulus to vessels exceeds the saturation point, so that the loss of one vasodilatory pathway does not further affect the vascular response (**Fig. S9**). This would also be consistent with isolated optogenetic or chemical stimulation of type-I nNOS neurons being able to drive substantial dilation, while the loss of these neurons does not have a large impact on the vascular response.

Finally, pharmacological ablation and optogenetic/chemogenetic activation are not mirror manipulations and have differences that can produce non-symmetrical changes. Symmetrical changes would only occur if the neural circuitry and the signaling to the vessel were completely linear. Optogenetic activation/deactivation of a single cell type does not produce symmetrical changes in the activity of other neurons (Phillips & Hasenstaub 2016), so there is little reason to think ablation would have the exact opposite effect as activation. Furthermore, optogenetic/pharmacological activation of a single cell type is unlikely to occur endogenously, as neural activity across different cell types is largely correlated (Bugeon et al 2022). For example, during whisker stimulation, not only are type-I nNOS neurons in the somatosensory cortex activated (Ruff et al 2024), but nearly every other cell type is as well (Staiger & Petersen 2021), which mean that type-I nNOS neurons are not the only neurons, and not even the only NO producing neurons, sending signals to the vasculature during sensory stimulation.

One surprise is that we observed no changes in the vasodilation during NREM sleep, where type-I nNOS neurons are known to be active and play a role in inducing sleep (Kilduff et al 2011). During NREM sleep, there is marked arterial dilation (Gheres et al 2023, Turner et al 2020), and it would seem natural that type-I nNOS neurons might drive this. However, we saw no difference in NREM dilation between the ablated and control mice. This could be due to compensation, saturation of the vasodilatory response, or it could be due to type-I nNOS neurons releasing other vasoconstrictory peptides (SST, NPY) so their net effects are cancelled out. This last possibility is consistent with the loss of the post-stimulus vasoconstriction seen after type-I nNOS neuron ablation. Again, like with sensory stimulation, there may be a non-linearity in the vascular responses, so that another large factor, such as large neuromodulatory changes during sleep, could dominate over any other vascular signaling factor. The large norepinephrine decreases during NREM (Kjaerby et al 2022, Osorio-Forero et al 2021, Turner et al 2023) could release the vessels from tonic vasoconstriction (as norepinephrine is a vasoconstrictor (Bekar et al 2012)), resulting in the dilation during NREM.

Finally, we saw a marked reduction in spontaneous vascular oscillation (vasomotion) at rest, both at the level of single arteries, and at the level of blood volume. These spontaneous oscillations move cerebrospinal fluid (CSF) (Holstein-Ronsbo et al 2023, Kedarasetti et al 2022, van Veluw et al 2020) which is important for clearing waste from the brain, and a reduction in amplitude will decrease the pumping efficacy. Additionally, there is a loss of coordination of neural and vascular dynamics across hemispheres after ablation of type-I nNOS neurons, indicated by the

drop in coherence. Although a loss of synchronous dilations/constrictions might affect CSF movement, we might imagine that it would also adversely impact CSF pumping. Aged human brains show reduced interhemispheric synchrony in resting-state signals (Zhao et al 2020), analogous to what we see here. Type-I nNOS neurons also seem uniquely vulnerable to stress (Han et al 2019), and loss of type-I nNOS neurons reduces power in the 1-4Hz band of the LFP, which is positively associated with CSF clearance (Hablitz et al 2019, Jiang-Xie et al 2024). It is possible that adverse life experiences could cause the loss of type-I nNOS neurons, leading to reduction in CSF flow seen in age (Kress et al 2014, Matrongolo et al 2023) that is thought to correlate with neurodegeneration.

Materials and Methods

This study was performed in accordance with the recommendations of the Guide for the Care and Use of Laboratory Animals of the National Institutes of Health. All procedures were performed in accordance with protocols approved by the Institutional Animal Care and Use Committee of Pennsylvania State University (Protocol 201042827). Data were acquired from 119 C57BL6/J mice (#000664, The Jackson Laboratory, Bar Harbor, ME) compromised of 57 males and 62 females between 3 and 9 months of age. Previous work from our lab has shown that the vasodilation elicited by whisker stimulation is the same in 2–4-month-old mice as in 18-month-old mice (Bennett et al 2024). As the age range used here is spanned by this time interval, we would not expect any age-related differences. Food and water were provided *ad libitum* and animals were housed on a 12-hr. light/dark cycle with all experiments occurring during the light cycle. Mice were individually housed after surgery. Sample sizes are consistent with previous studies (Echagarruga et al 2020, Turner et al 2023, Turner et al 2020, Zhang et al 2021) and based on a power analysis requiring 8-10 mice per group (Cohen's d = 1.3, $\alpha = 0.05$, $(1 - \beta) = 0.800$. Experimenters were not blind to experimental conditions or data analysis except for histological experiments. Two SP-SAP mice were removed from the imaging datasets (24 SP-SAP remaining) due to not showing ablation of nNOS neurons during post-histological analysis, an attrition rate of approximately 8%.

Surgical Procedures

Saporin is a ribosome-inactivating protein that was conjugated to the Sar^{9}, $Met(O_2)^{11}$ analog of Substance P (SP-SAP) or to a control peptide (Blank-SAP) (IT11 & IT21, Advanced Targeting Systems, Carlsbad, CA). Mice were anesthetized using 5% isoflurane (2% maintenance) vaporized in pure oxygen and were then injected intracortically with 4 ng of either SAP conjugate or Blank-SAP in 100 nL of artificial cerebrospinal fluid (aCSF). The incision site was sterilized with betadine and 70% ethanol followed by a retraction of the skin atop the skull. A small (< 0.5 mm) craniotomy was made above the vibrissae representation of somatosensory cortex (2 mm caudal, 3.25 mm lateral) and a sterile glass-pulled needle (tip diameter 50-100 μm) was inserted 500 μm beneath the cortical surface at 45°. The SAP conjugate was slowly injected at 100 nL/min using a programmable syringe pump (Harvard Apparatus, Holliston, MA) followed by closure of the incision with VetBond (3M, Saint Paul, MN). A subset of animals were also injected retro-orbitally with 25 μL of AAV PHP.eB-syn-jGCaMP7s-WPRE [2×10^{13} GC/mL] (104487-PHPeB, Addgene, Watertown, MA) diluted in 25 μL of sterile saline. Animals were given at least 2 weeks to recover prior to undergoing additional procedures. For imaging, a custom-machined titanium head bar was adhered atop the occipital bone of the skull using cyanoacrylate glue (Vibra-Tite 32402, ND Industries, Clawson, MI) and dental cement (Ortho-Jet, Lang Dental, Wheeling, IL). Self-tapping 3/32' #000 screws (J.I. Morris, Oxford, MA) were implanted in the frontal bones for structural stability. Electrodes were implanted into cortex and hippocampus using PFA-coated tungsten stereotrodes (#795500, AM systems, Sequim, WA) for recordings of local field potentials (LFP) and into the neck muscles using a pair of PFA-coated 7-strand stainless-steel wires (#793200, AM systems, Sequim, WA) for electromyography (EMG). Polished and reinforced thinned-skull

windows (Drew et al., 2010a; Shih et al., 2012b) were implanted over the somatosensory areas (either bilaterally or right hemisphere) using #0 coverslips (#72198, Electron Microscopy Sciences, Hatfield, PA). Detailed surgical procedures are as previously described (Turner et al 2020).

Data acquisition

Data were acquired with a custom LabVIEW program (National Instruments; *https://github.com/DrewLab/* LabVIEW-DAQ). Details on widefield optical imaging, two-photon microscopy, electromyography (EMG), electrophysiology, vibrissae stimulation, and behavioral measurements including tracking of vibrissae and pupil diameter were performed as previously described (Turner et al 2023, Turner et al 2020, Zhang et al 2022). Mice were gradually acclimated to head-fixation of increasing duration (15, 30, 60 minutes) on the days preceding the onset of experiments. The vibrissae (left, right, or a third air puffer not directed at the body as an auditory control) were randomly stimulated with air puffs [0.1 seconds or a train of 5 second pulses, 10 pounds force per square inch (PSI)] occurring every 30–45 seconds for the first 1 hour of imaging. Data were acquired in 15-minute intervals with a brief (~30 seconds) gap in between for saving data to disk. Each animal was run for up to 6 imaging sessions lasting from 1-5 hours depending on experiment. In two-photon experiments, mice were briefly anesthetized and retro-orbitally injected with 100 µL of 5% (weight/volume) fluorescein isothiocyanate–dextran (FITC) (FD150S, Sigma-Aldrich, St. Louis, MO) dissolved in sterile saline. Imaging was done on a Sutter Movable Objective Microscope with a CFI75 LWD 16X W objective (Nikon, Melville, NY) and a MaiTai HP Ti:sapphire laser (Spectra-Physics, Santa Clara, CA) tuned to 800 nm.

Histology

Following the conclusion of imaging experiments, animals were deeply anesthetized and transcardially perfused with heparin-saline followed by 4% paraformaldehyde. Presence or absence of nNOS-positive neurons in the injected hemisphere was verified using nicotinamide adenine dinucleotide phosphate (NADPH)-diaphorase staining for localizing the sparsely populated type-I nNOS neurons (Scherer-Singler et al 1983).

Immunohistochemistry

All histological analyses were done blinded to the experimental condition. Mice were deeply anesthetized with 5% isoflurane and perfused transcardially with ice-cold phosphate buffered saline (PBS, pH 7.4) and 4% paraformaldehyde (PFA, pH 7.4). Brains were removed, post-fixed in PFA for 24 hours and stored in PBS at 4°C for less than 1 week. A fiduciary mark was placed in the right hemisphere. 40-µm free floating sections were sliced with a Leica vibratome (VS 1200, Leica) and stored in PBS for less than 1 week. Prior to immunostaining, slices were washed three times in PBS for 10 minutes each and underwent antigen retrieval in 10 mM sodium citrate buffer (pH 6.0) at 80°C for 30 minutes. Slices were washed three times in PBS for 10 minutes each, and permeabilized in 0.5% Triton X-100 in PBS for 60 minutes. Nonspecific binding was blocked with 5% normal donkey serum (NDS) (ab7475) in 0.1% Triton X-100 in PBS for 60 minutes. Slices were then incubated in a primary antibody cocktail, including goat anti-nNOS (1:500, ab1376), rabbit anti-IBA-1 (1:500, ab178847), rat anti-GFAP (1:500, Thermofisher 13-0300), rabbit anti NeuN (1:2000, EnCor), rabbit anti-TACR1 (1:500 Invitrogen PA1-16713) in 2.5% NDS in 0.1% Triton X-100 in PBS for 48-h at 4°C. Slices were rinsed three times with PBS for 10 minutes each, and incubated in a fluorophore-tagged secondary antibody cocktail, including donkey anti-rabbit Alexa Fluor 488 (1:500, ab150073), donkey anti-goat Alexa Fluor 594 (1:500, ab150132), donkey anti rabbit Alexa fluor 647 (1:500, ab150075), donkey anti rat Alexa fluor 488 (1:500 ab150153), for 4 hours at room temperature. Slices were rinsed again three times with PBS, with the last step including DAPI (1:10,000, 10mg/mL, Millpore Sigma, 10236276001), mounted on glass slides, air-dried and cover slipped with Immunomount (Thermo Fisher Scientific, Waltham, MA, United States). Images were obtained with an Olympus BX63 upright microscope (Center Valley, PA, United States) under matched exposure settings. Three to eight images from both hemispheres were taken per region.

Cell counting and immunofluorescence quantification

Total cell counts and absolute changes in immunofluorescence (**Fig. 1**) were quantified using ImageJ (National Institutes of Health, Bethesda, MD, United States). The region of interest for analysis of cell counts was determined based on the injection site for both SP-SAP and Blank SAP injections, with a 1 mm diameter circle centered around the injection site and averaged across 3-5 sections where available. In most animals, the SP-SAP had a lateral spread greater than 500 microns and encompassed the entire depth of cortex (1-1.5 mm in SI). For total cell counts, a region of interest (ROI) was delineated, and cells were automatically quantified under matched criteria for size, circularity and intensity. Image threshold was adjusted until absolute value percentages were between 1-10% of the histogram density. The function *Analyze Particles* was then used to estimate the number of particles with a size of 100-99999 pixels^2 and a circularity between 0.3 and 1.0 (Dao et al 2020, Sicher et al 2023, Smith et al 2020). Immunoreactivity was quantified as mean fluorescence intensity of the ROI (Pleil et al 2015).

Data Analysis

Data were analyzed with code written by K.L.T, M.S.H, Q.Z, K.W.G, and P.J.D. (MATLAB 2019b–2024a, MathWorks).

Statistical analysis

Statistical evaluations were made using either generalized linear mixed effects (GLME), unpaired t-test, or general linear model (GLM). GLME models had the arousal state as a fixed effect, mouse identity as a random effect, and hemisphere [left/right (L/R), if applicable] as an interaction with the animal ID, or using a paired t test where appropriate. Unless otherwise stated, statistical results report p values from a GLME test. All reported quantifications are mean ± SD unless otherwise indicated. Unless otherwise noted, all pupil diameter measurements are in z-units. MATLAB functions used were fitglme, ttest, fitglm.

Hemodynamic correction

Widefield imaging was done with a Dalsa 1M60 Pantera CCD camera (Phase One, Cambridge, MA) with a magnifying lens (VZM 300i, Edmund Optics, Barrington, NJ). Reflectance measurements (**Fig. 2**) were converted to changes in total hemoglobin (Δ[HbT]), oxy-hemoglobin (Δ[HbO]), and deoxy-hemoglobin (Δ[HbR]) using the Beer–Lambert law (Ma et al., 2016a, b). Correction for attenuation of GCaMP7s fluorescence due to absorption of the surrounding tissue was corrected as previously described (Kramer & Pearlstein 1979, Ma et al 2016a, Scott et al 2018, Wright et al 2017). Changes in fluorescence intensity in the GCaMP7s signal due to blood absorption were approximated in a pixel-wise fashion by multiplying each value by the ratio of the green and blue channel's resting baseline pixel value.

Two-photon image processing

Image stacks were corrected for x-y motion artifacts and aligned with a rigid registration algorithm. A rectangular box was drawn around a straight, evenly-illuminated vessel segment and the pixel intensity was averaged along the long axis to calculate the vessel's diameter from the full-width at half-maximum (*https://github.com/DrewLab/Surface-Vessel-FWHM-Diameter*; (Drew et al 2011)). The diameter of penetrating arterioles was calculated using the thresholding in Radon space (TiRS) algorithm (*https://github.com/DrewLab/Thresholding_in_Radon_Space*; (Gao & Drew 2014, Gao et al 2015) .

Electrophysiology

Gamma-band [30–100Hz] LFP band was digitally bandpass filtered from recorded broadband data using a third-order Butterworth filter, squared, low-pass filtered below 1 Hz, and resampled at 30 Hz. Time-frequency spectrograms (**Fig. 2**) were calculated using the Chronux toolbox version 2.12 v03 (Bokil et al 2010), function mtspecgramc with a 5 s window and 1/5 s step size using [5,9] tapers and a passband of 1–100 Hz to encompass the LFP. EMG (300–3 kHz) from the neck muscles was bandpass filtered, squared, convolved with a Gaussian kernel with a standard deviation of 0.5 seconds, log transformed, then resampled at 30 Hz. MATLAB function(s): butter, zp2sos, filtfilt, gausswin, log10, conv, resample.

Evoked responses and slope

Evoked responses (**Fig. 3**) including whisker stimulation and locomotion for the various data types ([HbT], [HbO], [HbR], GCaMP7s, arteriole diameter) were compared between the indicated intervals (i.e., 2:4 seconds post-stimulation). The average of the 2 seconds preceding event onsets were subtracted from the event and smoothed with a 3rd order Savitzky-Golay filter. The average slope was calculated by comparing the rise (Δ[HbT]) over the run (neural data) before being fit with a linear model forced through the origin. MATLAB function(s): sgolayfilt)

Spectral power and coherence

Spectral power (**Fig. 4**, **5**, **6** **S5**) was estimated using the Chronux toolbox (Bokil et al 2010) function mtspectrumc. Data was detrended within individual events and truncated to the desired length depending on behavior (10 seconds for rest, 15 minutes for Alert and Asleep). Coherence analysis between two signals within the same hemisphere or between signals recorded bilaterally was run for each data type Chronux function coherencyc after detrending using the MATLAB function detrend.

Cross-correlation

Cross-correlations (**Fig. 5**) between gamma-band power or ΔF/F and changes in total hemoglobin Δ[HbT] were taken during periods of resting-state, alert, and asleep. Data were mean-subtracted and digitally lowpass filtered (< 1 Hz) with a fourth-order Butterworth filter (MATLAB function(s): butter, zp2sos, filtfilt). Cross-correlation analysis was run for each arousal state (MATLAB function(s): xcorr) with a ± 5 second lag time.

Resting-state variance and Δ[HbT] during different arousal states

Variance during the resting-state for both Δ[HbT] and diameter signals (**Fig. 7**) was taken from resting-state events lasting ≥10 seconds in duration. Average Δ[HbT] from within the 1 mm ROI over the vibrissae representation of SI during each arousal state was taken with respect to awake resting baseline events ≥10 seconds in duration. Continuous NREM sleep events ≥30 seconds, REM sleep events ≥60 seconds, and periods following administration of isoflurane were compared between groups. Each event was digitally lowpass filtered (<1 Hz) with a fourth-order Butterworth filter (MATLAB function(s): butter, zp2sos, filtfilt) and then averaged within each individual time series prior to comparing across animals/groups.

Open field behavior

Exploratory behavior (**Fig. S2**) was measured in a custom-made 30 cm x 60 cm arena during the light phase. Mice were not habituated to the arena. Mice were placed in the arena for 10 minutes to explore, and their behavior was recorded using an overhead camera (Blackfly BFLY-U3-23S6M, Teledyne FLIR, Wilsonville, OR) with 6 mm fixed focal length lens (Edmund Optics, Barrington, NJ, Stock #33939) at a frame rate of either 15 or 30 frames per second. The arena was illuminated with 780nm light. The surroundings of the arena were dark during the entire recording session. The

arena was cleaned with 70% ethanol in between animals. Only the first 5 minutes of the behavior were analyzed and reported here. The total distance traveled over the first 5 minutes, and the time spent in the 25 x 55 cm center rectangle was quantified. Generalized linear mixed effect (GLME) was used in MATLAB to perform statistical analysis. No statistical outliers were removed from the data. Mouse behavior was tracked using DeepLabCut (Mathis et al 2018) and analyzed with custom MATLAB algorithms (Brockway et al 2023, Zhang et al 2022). Eight points on the body (left ear, right ear, head, mid, back near the hip joint, base of the tail, midpoint of the tail, and end of the tail) were tracked. Four markers placed in the arena's four corners with an additional four points calculated from the four corners to track the center rectangle. A DeepLabCut model was trained and evaluated on a subset of mice before applying the model to all the mice. DeepLabCut tracking was considered acceptable if the tracking confidence was above 97%; however, in most cases, it was higher than 99%. Tracking positions were exported to a CSV file containing the tracked location's XY coordinates (frame pixels). Tracked videos from random mice were visualized to confirm the accuracy of the tracking. The experimenter was blinded to drug injection group identification until tracking and analysis were completed. The distance was calculated from the first 5 minutes as Euclidean distance between the point tracked in the middle of the mouse body from subsequent frames. Center time was quantified as the number of frames a mouse spends within the polygon bounded by 4 points tracked on the center of the arena.

Sleep scoring

Sleep scoring (**Fig. S3**) was performed as in Turner et al. (2020). Briefly, arousal state was scored using a combination of cortical and hippocampal LFP, EMG, pupil diameter, and whisker and body moment. Periods of manually chosen awake rest 5s in duration with no vibrissae or body motion were used as a baseline to normalize neural and hemodynamic signals. NREM sleep shows elevated cortical delta-band power and lower EMG power. REM sleep is marked by elevated hippocampal theta-band power and elevated cortical gamma-band power with very low baseline EMG power (muscle atonia; Cantero et al., 2004; Montgomery et al., 2008; Le Van Quyen et al., 2010; Sullivan et al., 2014). Every 5 second interval was classified as either Awake, NREM sleep, or REM sleep using a bootstrap aggregating random forest model with the predictors of cortical delta band power, cortical beta band power, cortical gamma LFP, hippocampal theta LFP, EMG power, heart rate, and whisking duration. Sleep model accuracy was validated using the out-of-bag error during model training. MATLAB functions used were TreeBagger, oobError, predict.

Pupil diameter and interblink interval

Pupil diameter (**Fig. S2**) was lowpass filtered at 1 Hz with a fourth-order Butterworth filter. Changes in whisking-evoked and stimulus-evoked (contralateral, auditory) diameters normalized relative to the mean of the 2 second preceding the event onset. MATLAB functions used were butter, zp2sos, filtfilt. Interblink interval and blink-associated physiology. Because of breaks in recording to save the data to disk, interblink interval was calculated between blinks occurring within 15 min records and not blinks on the edges of trials. Blinks that occurred within 1 second of each other were linked together as blinking bouts, and all blink-triggered analyses were with respect to the first blink in a series. Blink-triggered averages were separated into two groups depending on the arousal state classification of the 5 second bin before the blink, being either Awake (arousal state classification of Awake) or Asleep (arousal state classification being either NREM or REM).

Hemodynamic response function

The hemodynamic response function (HRF, **Fig. S5**) was calculated as previously described (Winder et al 2017, Zhang et al 2023) using both deconvolution and fitting the response to a gamma distribution. Only neural activity (gamma-band power, 30-100 Hz) within 1.5 second of the stimulus was used for calculating the HRF. Each HRF was calculated using half of the data and tested on the other half. To test the predictive capability of each HRF, the impulse function was fit

with a gamma-distribution function and convolved with the neural power to predict the measured hemodynamic signal. The coefficient of determination (R^2) between the predicted and actual hemodynamic signal was evaluated to quantify the efficacy of HRF's prediction (MATLAB function(s): sgolayfilt, detrend, fminsearch, fitlm).

Pearson's correlation coefficient calculations

The Pearson's correlation coefficient between bilateral signals (**Fig. S6**) was obtained by mean-subtracting and digitally lowpass filtering (<1 Hz) with a fourth-order Butterworth filter and then taking the Pearson's correlation coefficient (MATLAB function(s): butter, zp2sos, filtfilt, corrcoef).

Arousal state transitions

Transitions between arousal states (Awake to NREM, NREM to Awaken, NREM to REM, REM to Awake) were compared across groups (**Fig. S8**) by averaging events that met the criteria of 30 seconds of one state's consecutive classifications followed by 30 seconds of another state. The difference in the Δ[HbT] between the pre- and post-state transition were compared by taking the 30:10 seconds prior to the transition zero point to the 10:30 seconds following. [HbT] was digitally lowpass (<1 Hz) filtered using a fourth-order Butterworth filter (MATLAB function(s): butter, zp2sos, filtfilt).

Data availability

Data and code for generating the figures are available at *http://doi.org/10.5061/dryad.tb2rbp0bq* and analysis code is available at *https://github.com/KL-Turner/Turner-eLife2025*. Raw data is available upon reasonable request.

Figure supplements

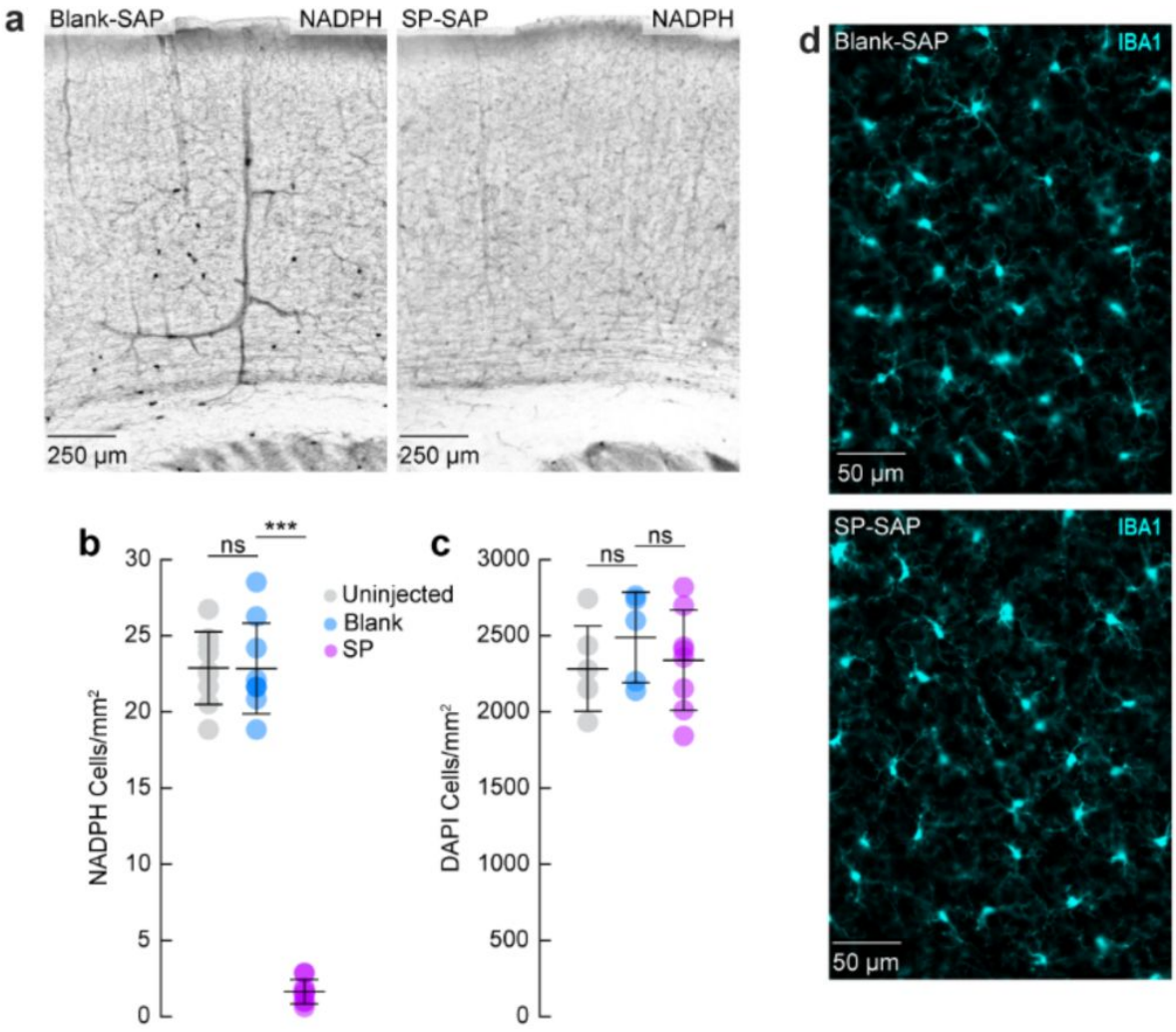

Figure S1.

Histological quantification of cortical SP-Sap injections

(a) Examples of NADPH diaphorase staining from Blank-SAP and SP-SAP injected mice. **(b)** SP-SAP injected mice (N = 9, 5M/4F) had significantly lower numbers of type-I nNOS cells than either Blank-SAP (N = 9, 4M/5F) or Uninjected mice (N = 9, 4M/5F) (SP-SAP: 1.6 ± 0.8 neurons/mm^2; Blank-SAP: 22.9 ± 2.4 neurons/mm^2; Uninjected: 22.9 ± 3 neurons/mm^2; Blank-SAP vs. Uninjected: p = 0.98; Blank-SAP vs. SP-SAP: p = 2.23×10^{-13}). **(c)** Counts of DAPI-labeled cell nuclei per square mm from imaged mice. Uninjected (N = 6, 6M) mice had 2284 ± 279 DAPI-labeled cell bodies/mm^2, which was not significantly different than those injected with Blank-SAP (N = 5, 5F, 2488 ± 298, p = 0.23, GLME), which in turn was not significantly different than those injected with SP-SAP (N = 8, 4M/4F, 2340 ± 329, p = 0.39, GLME. **(d)** Representative image of IBA1 for Blank-SAP (top) and SP-SAP (bottom) taken from **Fig 1c**. Error bars (**b, c**) denote SD. *α < 0.05, **α < 0.01, ***α < 0.001, GLME.

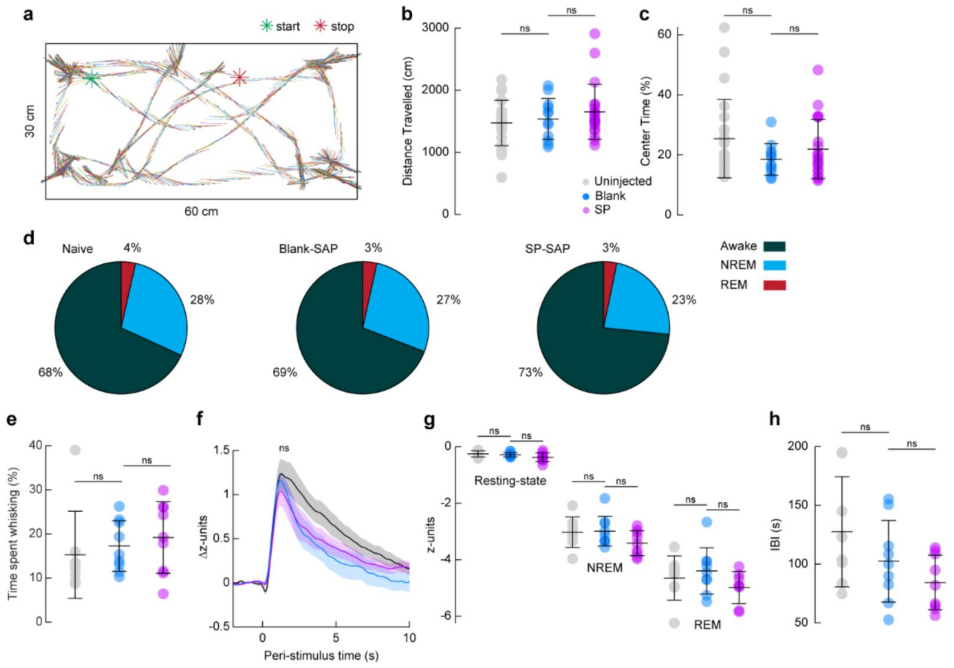

Figure S2.

Behavior was unaffected by local ablation of type-I nNOS neurons

(a) Example of exploratory behavior during 5 minutes of exploration in a novel environment. **(b)** Total distance traveled during open field exploration. Uninjected mice traveled an average of 1473.4 ± 364.7 cm compared with 1536.6 ± 329.6 cm in Blank-SAP (p = 0.61) and 1652.3 ± 442.7 cm in SP-SAP (p = 0.43). **(c)** Time spent in the center of the open field. Uninjected mice spent on average 25.5 ± 13.1% of total exploration time in the center compared with 18.5 ± 5.3% in Blank-SAP (p = 0.08, GLME) and 21.9 ±9.8% in SP-SAP (p = 0.26). **(b, c)** n = 12-23 mice per group. **(d)** Percentage of time classified in each arousal state by sleep scoring. Uninjected mice spent 68.1 ± 13.2% of the time awake compared to 69.1 ± 15.1% in Blank-SAP (p = 0.89, ttest) and 73.4 ± 11.6% in SP-SAP (p = 0.51, ttest). Uninjected mice spent 28.3 ± 11.1% of the time in NREM sleep compared to 27.4 ± 12.0% in Blank-SAP (p = 0.87, ttest) and 23.4 ± 9.7% in SP-SAP (p = 0.44, ttest). Uninjected mice spent 3.5 ± 2.9% of the time in REM sleep compared to 3.4 ± 3.5% in Blank-SAP (p = 0.96, ttest) and 3.2 ± 2.3% in SP-SAP (p = 0.88, ttest). **(e)** Time spent whisking as a percentage of total imaging time. Uninjected mice spent 15.3 ± 9.9% compared with 17.3 ± 5.8% in Blank-SAP (p = 0.61, ttest) and 19.2 ± 8.1% in SP-SAP (p = 0.75, ttest). **(f)** Change in Pupil diameter in response to vibrissae stimulation. Pupil diameter of uninjected mice increased 1.3 ± 0.5 z-units following vibrissae stimulation compared with 1.2 ± 0.3 z-units in Blank-SAP (p = 0.76, ttest) and 1.1 ± 0.5 z-units in SP-SAP (p = 0.50, ttest). **(g)** Average pupil diameter across arousal states. Average pupil diameter of Uninjected mice during the resting-state was −0.25 ± 0.1 z-units compared with −0.29 ± 0.1 z-units in Blank-SAP (p = 0.45, ttest) and − 0.34 ± 0.2 in SP-SAP (p = 0.14, ttest). Average pupil diameter of Uninjected mice during periods of NREM sleep was −3 ± 0.5 z-units compared with −3 ± 0.5 z-units in Blank-SAP (p = 0.89, ttest) and −3.4 ± 0.4 in SP-SAP (p = 0.08, ttest). Average pupil diameter of Uninjected mice during periods of REM sleep was −4.6 ± 0.8 z-units compared with −4.4 ± 0.8 z-units in Blank-SAP (p = 0.53, ttest) and −5 ± 0.6 in SP-SAP (p = 0.11, ttest) **(h)** Interblink-interval. Uninjected mice had a mean interblink-interval of 127.6 ± 46.8 s compared with 102.5 ± 34.7 s in Blank-SAP (p = 0.22, ttest) and 84.5 ± 23.3 s in SP-SAP (p = 0.21, ttest). **(d-h)** n = 9 mice per group. Shading **(f)** indicates SEM and error bars **(b, c, e, g, h)** denote SD. *α < 0.05, **α < 0.01, ***α < 0.001.

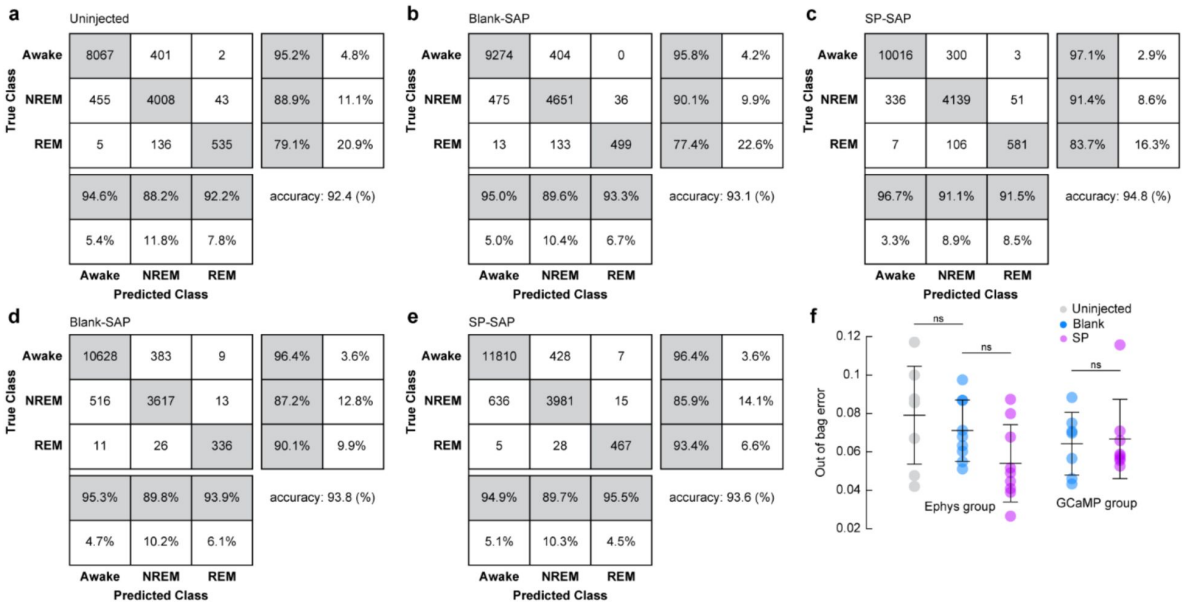

Figure S3.

Sleep classification accuracy was unchanged following type-I nNOS ablation

(a) Confusion matrix for arousal state classification of Uninjected mice with bilaterally implanted stereotrodes. **(b)** Confusion matrix for arousal state classification of Blank-SAP mice with bilaterally implanted stereotrodes. **(c)** Confusion matrix for arousal state classification of SP-SAP mice with bilaterally implanted stereotrodes. **(a-c)** n = 9 mice per group. **(d)** Confusion matrix for arousal state classification of Blank-SAP mice expressing pan-neuronal GCaMP. **(e)** Confusion matrix for arousal state classification of SP-SAP mice expressing pan-neuronal GCaMP. **(d, e)** n = 6-7 mice per group. **(f)** Out-of-bag error during training of each animal's bootstrapped random forest classification algorithm. For mice with bilateral LFP recordings, Uninjected mice had an average loss of 0.08 ± 0.03 in comparison to 0.07 ± 0.02 in Blank-SAP (p = 0.45, ttest) compared to 0.05 ± 0.02 in SP-SAP (p = 0.064, ttest). Blank-SAP mice with pan-neuronal GCaMP had an average classification loss of 0.06 ± 0.02 compared with 0.07 ± 0.02 in SP-SAP (p = 0.80, ttest). Error bars denote SD. *α < 0.05, **α < 0.01, ***α < 0.001.

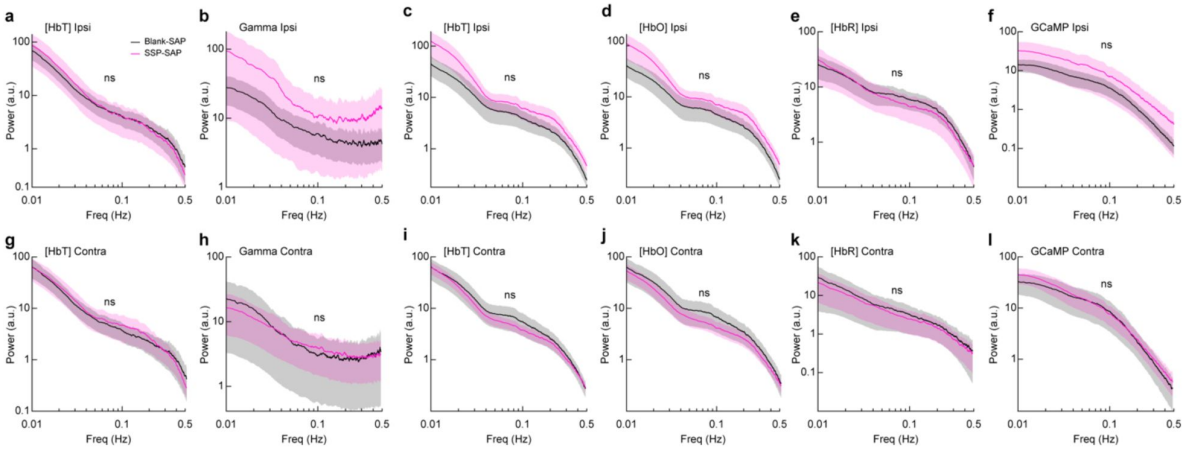

Figure S4.

Ablation of Type-I nNOS neurons does not alter hemodynamic or neural power spectra

Power spectral density for vascular and hemodynamic signals for the Blank-SAP group (N = 9, 4M/5F for **a, b, g, h**; N = 7, 3M/4F for **c-f; i-l**) and SP-SAP group (N = 9, 5M/4F for **a, b, g, h;** N = 8, 4M/4F for **c-f; i-l**) was not significantly different across all measurements of hemodynamic and neural signals in the injected (ipsilateral) hemisphere **(a-f)** or in the un-injected (contralateral) hemisphere **(g-l)**. **(a)** Δ[HbT] for electrophysiology animals (p = 0.65, GLME). **(b)** Gamma-band power (second spectra) for animals with electrophysiology (p = 0.47, GLME). **(c)** Δ[HbT] for animals with GCaMP (p = 0.27, GLME). **(d)** Δ[HbT] for animals with GCaMP (p = 0.27, GLME). **(e)** Δ[HbT] for animals with GCaMP (p = 0.97, GLME). **(f)** GCaMP fluorescence (p = 0.48, GLME). **(g)** Δ[HbT] for electrophysiology animals (p = 0.80, GLME). **(h)** Gamma-band power (second spectra) for animals with electrophysiology (p = 0.95, GLME). **(i)** Δ[HbT] for animals with GCaMP (p = 0.83, GLME). **(j)** Δ[HbT] for animals with GCaMP (p = 0.69, GLME). **(k)** Δ[HbT] for animals with GCaMP (p = 0.87, GLME). **(l)** GCaMP fluorescence (p = 0.82, GLME). Shading represents population averages ± SEM. *α < 0.05, **α < 0.01, ***α < 0.001.

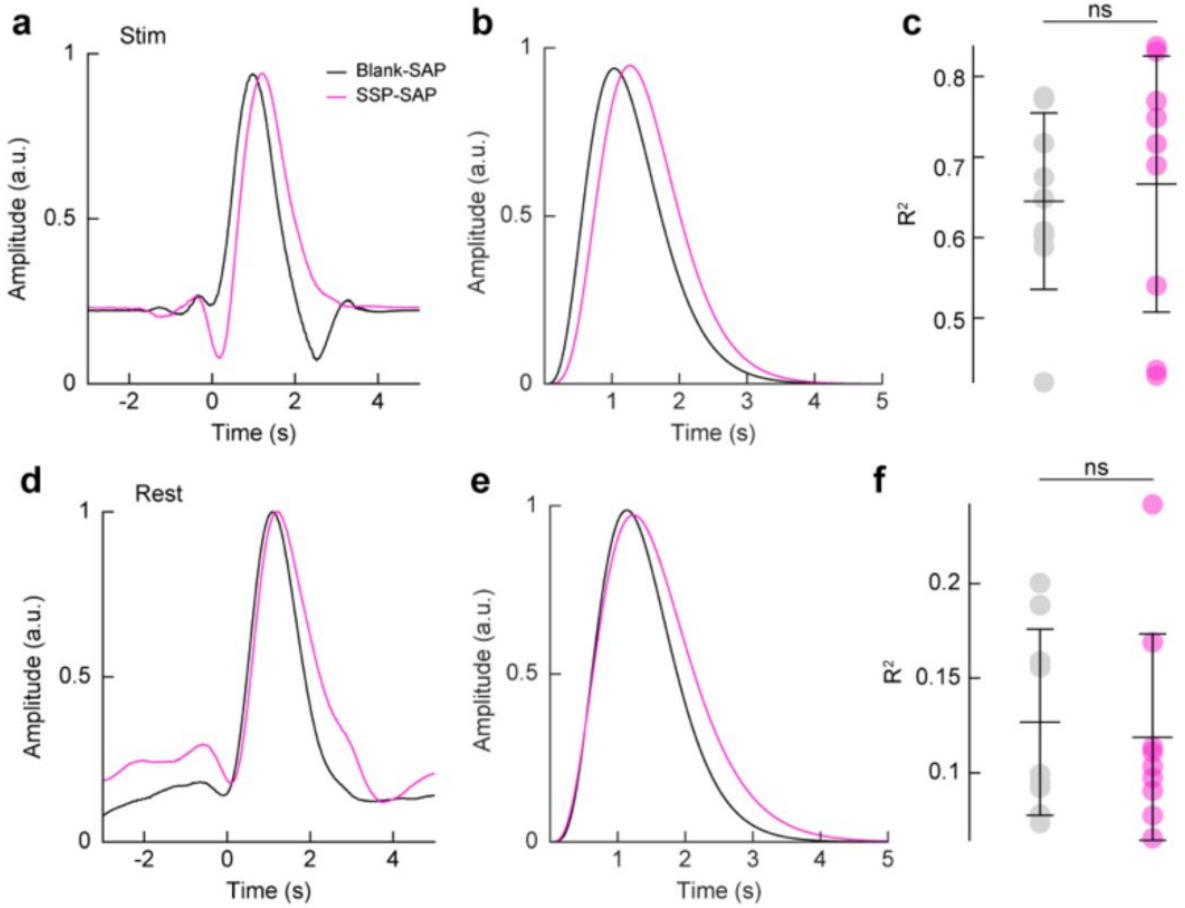

Figure S5.

Ablation of Type-I nNOS neurons does not alter the predictive power of the hemodynamic response function

(a) Stimulus-evoked hemodynamic response function obtained with deconvolution. **(b)** Stimulus-evoked hemodynamic response function fitted with a gamma distribution function. **(c)** There was no significant difference between the Δ[HbT] predictive R^2 values calculated from impulse-derived HRFs between Blank-SAP (N = 9, 4M/5F) 0.64 ± 0.11 or SP-SAP (N = 9, 5M/4F) 0.67 ± 0.16 following vibrissae stimulation (p = 0.746, ttest). **(d)** Resting-state hemodynamic response function based on deconvolution. **(e)** Resting-state hemodynamic response function fitted with a gamma distribution function. **(f)** There was no significant difference between the Δ[HbT] predictive R^2 values calculated from impulse-derived HRFs between Blank-SAP (N = 9, 4M/5F) 0.13 ± 0.0.05 or SP-SAP (N = 9, 5M/4F) 0.12 ± 0.05 during the resting-state (p = 0.749, ttest). Error bars denote SD. *α < 0.05, **α < 0.01, ***α < 0.001.

Figure S6.

Pearson's correlation coefficients between bilateral hemodynamic and neural signals

(a) Correlation coefficient between bilateral hemodynamic signals during the resting-state was 0.75 ± 0.04 in Blank-SAP and 0.68 ± 0.06 in SP-SAP (ttest p = 0.011), during the alert state was 0.85 ± 0.03 with Blank-SAP and 0.81 ± 0.06 in SP-SAP (ttest p = 0.09), and during the asleep state was 0.95 ± 0.02 in Blank-SAP and 0.92 ± 0.03 in SP-SAP (ttest p = 0.01). **(b)** Correlation coefficient between bilateral gamma-band power signals during the resting-state was 0.15 ± 0.04 in Blank-SAP and 0.14 ± 0.12 in SP-SAP (ttest p = 0.69), during the alert state was 0.23 ± 0.08 in Blank-SAP and 0.19 ± 0.11 in SP-SAP (ttest p = 0.31), and during the asleep state was 0.50 ± 0.08 in Blank-SAP and 0.41 ± 0.08 in SP-SAP (ttest p = 0.04). **(c)** Correlation coefficient between bilateral hemodynamic signals (GCaMP7s group) during the resting-state was 0.82 ± 0.04 in Blank-SAP and 0.75 ± 0.04 in SP-SAP (ttest p = 0.01), during the alert state was 0.93 ± 0.02 in Blank-SAP and 0.91 ± 0.02 in SP-SAP (ttest p = 0.08), and during the asleep state was 0.98 ± 0.02 with SP-SAP and 0.95 ± 0.03 in SP-SAP (ttest p = 0.07). **(d)** Correlation coefficient between bilateral GCaMP7s signals during the resting-state was 0.70 ± 0.05 in Blank-SAP and 0.65 ± 0.09 in SP-SAP (ttest p = 0.16), during the alert state was 0.93 ± 0.03 with Blank-SAP and 0.92 ± 0.03 in SP-SAP (ttest p = 0.31), and during the asleep state was 0.96 ± 0.02 with Blank-SAP and 0.95 ± 0.02 in SP-SAP (ttest p = 0.37). Error bars denote SD. $\alpha < 0.05$, $**\alpha < 0.01$, $***\alpha < 0.001$.

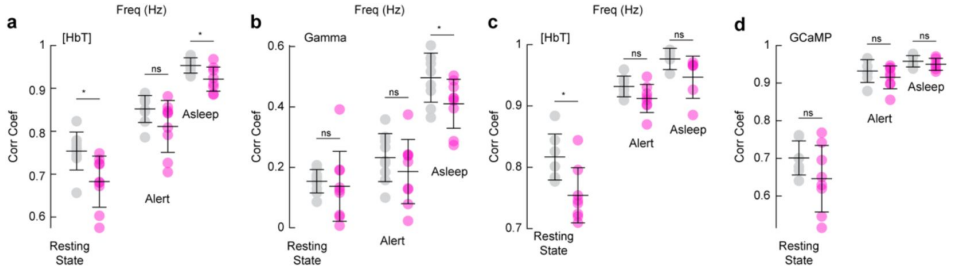

Figure S7.

Ablation of Type-I nNOS neurons does not alter LFP or vasomotion in the contralateral hemisphere

(a) The power in the delta-band of the LFP in Blank-SAP mice (N = 9, 4M/5F) in the alert state (**Fig. 4a**) was 1.6×10^{-10} ± 2.4×10^{-11} a.u. compared to 2.1×10^{-10} ± 2.5×10^{-11} a.u. in the SP-SAP mice (N = 9, 5M/4F, GLME p = 0.14). **(b)** The power in the delta-band of the LFP in Blank-SAP mice (N = 7, 3M/4F) in the asleep state was (NREM + REM) was 3.2×10^{-10} ± 3.3×10^{-11} a.u. compared to 4.4×10^{-10} ± 9.7×10^{-11} a.u. in the SP-SAP mice (N = 7, 4M/3F, GLME p = 0.18). **(c)** The power in the delta-band of the LFP in Blank-SAP mice (N = 9, 4M/5F) averaged across all arousal states was 2.1×10^{-10} ± 3.1×10^{-10} a.u. compared to 3.1×10^{-10} ± 5.0×10^{-11} a. u. in the SP-SAP mice (N = 9, 5M/4F, GLME p = 0.11). **(d)** The variance in Δ[HbT] during rest, a measure of vasomotion amplitude, was not significantly reduced in the un-injected (contralateral) hemisphere following type-I nNOS ablation; dropping from 36.9 ± 3.4 μM^2 in the Blank-SAP group (N = 16, 7M/9F) to 28.2 ± 2.9 μM^2 in the SP-SAP group (N = 17, 9M/8F) (GLME p = 0.06). Shading represents population averages ± SEM. $*\alpha < 0.05$, $**\alpha < 0.01$, $***\alpha < 0.001$.

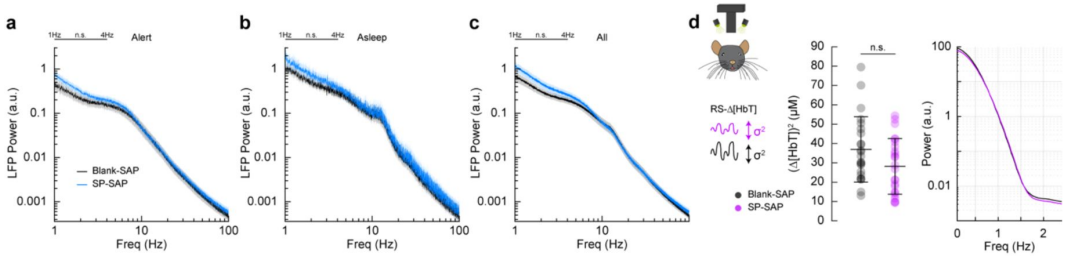

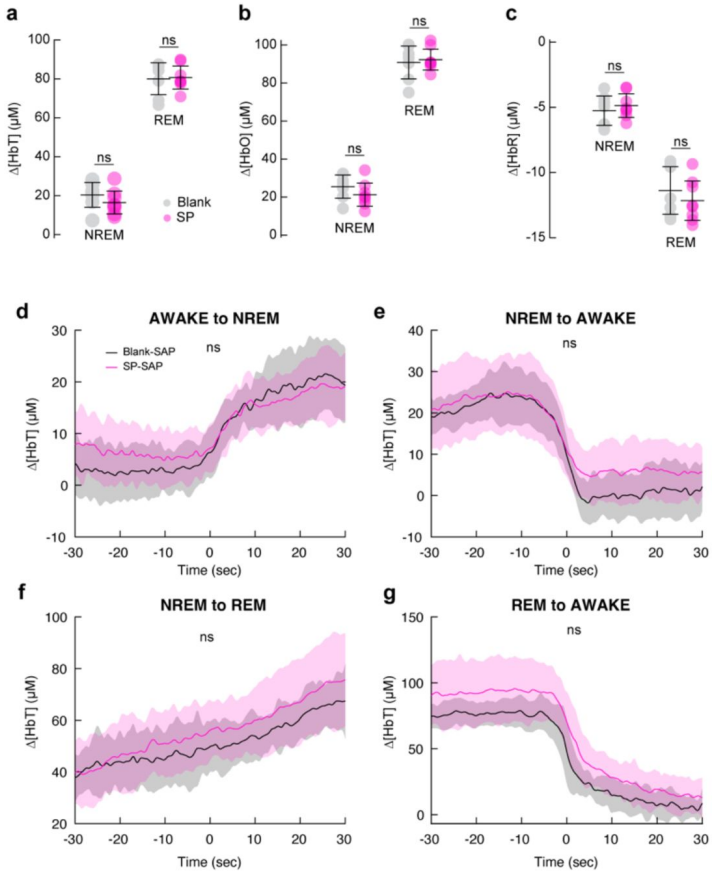

Figure S8.

Removal of type-I nNOS neurons did not alter arousal state-related hemodynamic changes (a-c)

Average Δ[HbT/O/R] during periods of NREM sleep and REM sleep in mice with pan-neuronal GCaMP (n = 6-7 mice per group). **(a)** NREM Δ[HbT] in Blank-SAP mice was 20.4 ± 6.4 μM compared to 16.5 ± 5.9 μM in SP-SAP (p = 0.27, ttest). REM Δ[HbT] in Blank-SAP mice was 80.0 ± 8.2 μM compared to 80.7 ± 5.9 μM in SP-SAP (p = 0.87, ttest). **(b)** NREM Δ[HbO] in Blank-SAP mice was 25.5 ± 6.1 μM compared to 21.2 ± 6.1 μM in SP-SAP (p = 0.23, ttest). REM Δ[HbO] in Blank-SAP mice was 90.8 ± 8.6 μM compared to 92.3 ± 5.5 μM in SP-SAP (p = 0.72, ttest). **(c)** NREM Δ[HbR] in Blank-SAP mice was −5.3 ± 1.1 μM compared to −4.9 ± 0.9 μM in SP-SAP (p = 0.50, ttest). REM Δ[HbR] in Blank-SAP mice was −11.4 ± 1.8 μM compared to −12.2 ± 1.5 μM in SP-SAP (p = 0.42, ttest). **(d)** Transition from Awake to NREM had a Δ[HbT] of −16.6 ± 6.4 μM in Blank-SAP mice and −11.1 ± 7.0 μM in SP-SAP mice (p < 0.08, GLME). **(e)** Transition from NREM to Awake had a Δ[HbT] of 21.5 ± 7.7 μM in Blank-SAP mice and 17.6 ± 9.5 μM in SP-SAP mice (p < 0.33, GLME). **(f)** Transition from NREM to REM had a Δ[HbT] of −17.6 ± 3.9 μM in Blank-SAP mice and −22.6 ± 7.9 μM in SP-SAP mice (p < 0.09, GLME). **(g)** Transition from REM to Awake had a Δ[HbT] of 67.8 ± 7.3 μM in Blank-SAP mice and 74.0 ± 13.1 μM in SP-SAP mice (p < 0.21, GLME). Error bars denote SD. Shading represents population averages ± SEM.*α < 0.05, **α < 0.01, ***α < 0.001.

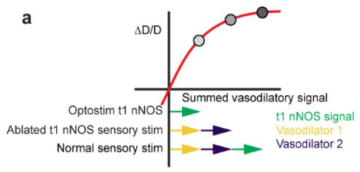

Figure S9.

Schematic showing how non-linearity in the dilation response can explain coexistence strong dilation by activation of a pathway, and little change after weakening a pathway.

If the diameter is a sublinear function of the sum of vasodilatory inputs, activation of all pathways will cause a dilation that is smaller than the sum of activation of each pathway individually. Loss of one pathway will not cause large changes, even though activation of that pathway in isolation can cause large dilations.

Acknowledgements

This work was supported by NIH Grants R01NS078168, R01NS079737, U19NS128613 to PJD, R01AA029403 to NAC, an American Heart Association Predoctoral fellowship 24PRE1201066 to MSH and F31ES036154 to DIG. DIG was supported by T32GM108563 and MSH was supported by T32NS115667.

Additional information

Author Contributions

K.L.T, N.A.C, and P.J.D. designed the experiments. K.L.T, D.F.B, M.S.H, K.R.G, D.I.G, and Q.Z performed experiments. K.L.T., M.S.H, Q.Z, K.W.G., and P.J.D. analyzed the data. K.L.T. and P.J.D. wrote the paper.

Funding

National Institutes of Health (R01NS078168)

National Institutes of Health (R01NS079737)

National Institutes of Health (U19NS128613)

National Institutes of Health (R01AA029403)

National Institutes of Health (F31ES036154)

National Institutes of Health (T32GM108563)

American Heart Association

https://doi.org/10.58275/aha.24pre1201066.pc.gr.190598

References

Abbott SB, Kanbar R, Bochorishvili G, Coates MB, Stornetta RL, Guyenet PG (2012) **C1 neurons excite locus coeruleus and A5 noradrenergic neurons along with sympathetic outflow in rats** *J Physiol* **590**:2897–915 Google Scholar

Ahn SJ, Anfray A, Anrather J, Iadecola C (2023) **Calcium transients in nNOS neurons underlie distinct phases of the neurovascular response to barrel cortex activation in awake mice** *J Cereb Blood Flow Metab* :271678X Google Scholar

Andrei AR, Debes S, Chelaru M, Liu X, Rodarte E, et al. (2021) **Heterogeneous side effects of cortical inactivation in behaving animals** *eLife* :10 Google Scholar

Attwell D, Buchan AM, Charpak S, Lauritzen M, Macvicar BA, Newman EA (2010) **Glial and neuronal control of brain blood flow** *Nature* **468**:232–43 Google Scholar

Bekar LK, Wei HS, Nedergaard M (2012) **The locus coeruleus-norepinephrine network optimizes coupling of cerebral blood volume with oxygen demand** *Journal of Cerebral Blood Flow & Metabolism* **32**:2135–45 Google Scholar

Bennett HC, Zhang Q, Wu YT, Manjila SB, Chon U, et al. (2024) **Aging drives cerebrovascular network remodeling and functional changes in the mouse brain** *Nat Commun* **15**:6398 Google Scholar

Bergamaschi G, Perfetti V, Tonon L, Novella A, Lucotti C, et al. (1996) **Saporin, a ribosome-inactivating protein used to prepare immunotoxins, induces cell death via apoptosis** *Br J Haematol* **93**:789–94 Google Scholar

Bokil H, Andrews P, Kulkarni JE, Mehta S, Mitra PP (2010) **Chronux: a platform for analyzing neural signals** *J Neurosci Methods* **192**:146–51 Google Scholar

Bredt DS, Glatt CE, Hwang PM, Fotuhi M, Dawson TM, Snyder SH (1991) **Nitric oxide synthase protein and mRNA are discretely localized in neuronal populations of the mammalian CNS together with NADPH diaphorase** *Neuron* **7**:615–24 Google Scholar

Brockway DF, Griffith KR, Aloimonos CM, Clarity TT, Moyer JB, et al. (2023) **Somatostatin peptide signaling dampens cortical circuits and promotes exploratory behavior** *Cell Rep* **42**:112976 Google Scholar

Bugeon S, Duffield J, Dipoppa M, Ritoux A, Prankerd I, et al. (2022) **A transcriptomic axis predicts state modulation of cortical interneurons** *Nature* **607**:330–38 Google Scholar

Cardin JA, Carlen M, Meletis K, Knoblich U, Zhang F, et al. (2009) **Driving fast-spiking cells induces gamma rhythm and controls sensory responses** *Nature* **459**:663–7 Google Scholar

Chan KY, Jang MJ, Yoo BB, Greenbaum A, Ravi N, et al. (2017) **Engineered AAVs for efficient noninvasive gene delivery to the central and peripheral nervous systems** *Nat Neurosci* **20**:1172–79 Google Scholar

Chong PS, Poon CH, Fung ML, Guan L, Steinbusch HWM, et al. (2019) **Distribution of neuronal nitric oxide synthase immunoreactivity in adult male Sprague-Dawley rat brain** *Acta Histochem* **121**:151437 Google Scholar

Claron J, Provansal M, Salardaine Q, Tissier P, Dizeux A, et al. (2023) **Co-variations of cerebral blood volume and single neurons discharge during resting state and visual cognitive tasks in non-human primates** *Cell Rep* **42**:112369 Google Scholar

Dana H, Sun Y, Mohar B, Hulse BK, Kerlin AM, et al. (2019) **High-performance calcium sensors for imaging activity in neuronal populations and microcompartments** *Nat Methods* **16**:649–57 Google Scholar

Dao NC, Suresh Nair M, Magee SN, Moyer JB, Sendao V, et al. (2020) **Forced Abstinence From Alcohol Induces Sex-Specific Depression-Like Behavioral and Neural Adaptations in Somatostatin Neurons in Cortical and Amygdalar Regions** *Front Behav Neurosci* **14**:86 Google Scholar

Dittrich L, Heiss JE, Warrier DR, Perez XA, Quik M, Kilduff TS (2012) **Cortical nNOS neurons co-express the NK1 receptor and are depolarized by Substance P in multiple mammalian species** *Front Neural Circuits* **6**:31 Google Scholar

Dittrich L, Morairty SR, Warrier DR, Kilduff TS (2015) **Homeostatic sleep pressure is the primary factor for activation of cortical nNOS/NK1 neurons** *Neuropsychopharmacology* **40**:632–9 Google Scholar

Drew PJ (2019) **Vascular and neural basis of the BOLD signal** *Curr Opin Neurobiol* **58**:61–69 Google Scholar

Drew PJ, Shih AY, Driscoll JD, Knutsen PM, Blinder P, et al. (2010) **Chronic optical access through a polished and reinforced thinned skull** *Nat Methods* **7**:981–4 Google Scholar

Drew PJ, Shih AY, Kleinfeld D (2011) **Fluctuating and sensory-induced vasodynamics in rodent cortex extend arteriole capacity** *Proc Natl Acad Sci U S A* **108**:8473–8 Google Scholar

Drew PJ, Winder AT, Zhang Q (2019) **Twitches, Blinks, and Fidgets: Important Generators of Ongoing Neural Activity** *Neuroscientist* **25**:298–313 Google Scholar

Echagarruga CT, Gheres KW, Norwood JN, Drew PJ (2020) **nNOS-expressing interneurons control basal and behaviorally evoked arterial dilation in somatosensory cortex of mice** *eLife* :9 Google Scholar

Endo T, Yanagawa Y, Komatsu Y (2016) **Substance P Activates Ca2+-Permeable Nonselective Cation Channels through a Phosphatidylcholine-Specific Phospholipase C Signaling Pathway in nNOS-Expressing GABAergic Neurons in Visual Cortex** *Cereb Cortex* **26**:669–82 Google Scholar

Gao YR, Drew PJ (2014) **Determination of vessel cross-sectional area by thresholding in Radon space** *J Cereb Blood Flow Metab* **34**:1180–7 Google Scholar

Gao YR, Greene SE, Drew PJ (2015) **Mechanical restriction of intracortical vessel dilation by brain tissue sculpts the hemodynamic response** *Neuroimage* **115**:162–76 Google Scholar

Gerashchenko D, Schmidt MA, Zielinski MR, Moore ME, Wisor JP (2018) **Sleep State Dependence of Optogenetically evoked Responses in Neuronal Nitric Oxide Synthase-**

positive Cells of the Cerebral Cortex *Neuroscience* **379**:189–201 Google Scholar

Gerashchenko D, Wisor JP, Burns D, Reh RK, Shiromani PJ, et al. (2008) **Identification of a population of sleep-active cerebral cortex neurons** *Proc Natl Acad Sci U S A* **105**:10227–32 Google Scholar

Gheres KW, Unsal HS, Han X, Zhang Q, Turner KL, et al. (2023) **Arousal state transitions occlude sensory-evoked neurovascular coupling in neonatal mice** *Commun Biol* **6**:738 Google Scholar

Goense J, Merkle H, Logothetis NK (2012) **High-resolution fMRI reveals laminar differences in neurovascular coupling between positive and negative BOLD responses** *Neuron* **76**:629–39 Google Scholar

Hablitz LM, Vinitsky HS, Sun Q, Staeger FF, Sigurdsson B, et al. (2019) **Increased glymphatic influx is correlated with high EEG delta power and low heart rate in mice under anesthesia** *Sci Adv* **5**:eaav5447 Google Scholar

Han K, Min J, Lee M, Kang BM, Park T, et al. (2019) **Neurovascular Coupling under Chronic Stress Is Modified by Altered GABAergic Interneuron Activity** *J Neurosci* **39**:10081–95 Google Scholar

Haselden WD, Kedarasetti RT, Drew PJ (2020) **Spatial and temporal patterns of nitric oxide diffusion and degradation drive emergent cerebrovascular dynamics** *PLoS Comput Biol* **16**:e1008069 Google Scholar

He M, Tucciarone J, Lee S, Nigro MJ, Kim Y, et al. (2016) **Strategies and Tools for Combinatorial Targeting of GABAergic Neurons in Mouse Cerebral Cortex** *Neuron* **91**:1228–43 Google Scholar

Hendry SH, Schwark HD, Jones EG, Yan J (1987) **Numbers and proportions of GABA-immunoreactive neurons in different areas of monkey cerebral cortex** *J Neurosci* **7**:1503–19 Google Scholar

Higo S, Udaka N, Tamamaki N (2007) **Long-range GABAergic projection neurons in the cat neocortex** *J Comp Neurol* **503**:421–31 Google Scholar

Hill CE (2012) **Long Distance Conduction of Vasodilation: A Passive or Regenerative Process?** *Microcirculation* **19**:379–90 Google Scholar

Holstein-Ronsbo S, Gan Y, Giannetto MJ, Rasmussen MK, Sigurdsson B, et al. (2023) **Glymphatic influx and clearance are accelerated by neurovascular coupling** *Nat Neurosci* Google Scholar

Hope BT, Michael GJ, Knigge KM, Vincent SR (1991) **Neuronal NADPH diaphorase is a nitric oxide synthase** *Proc Natl Acad Sci U S A* **88**:2811–4 Google Scholar

Hope BT, Vincent SR (1989) **Histochemical characterization of neuronal NADPH-diaphorase** *J Histochem Cytochem* **37**:653–61 Google Scholar

Hosford PS, Gourine AV (2019) **What is the key mediator of the neurovascular coupling response?** *Neurosci Biobehav Rev* **96**:174–81 Google Scholar

Huang H, Kuzirian MS, Cai X, Snyder LM, Cohen J, et al. (2016) **Generation of a NK1R-CreER knockin mouse strain to study cells involved in Neurokinin 1 Receptor signaling** *Genesis* **54**:593–601 Google Scholar

Huber L, Goense J, Kennerley AJ, Trampel R, Guidi M, et al. (2015) **Cortical lamina-dependent blood volume changes in human brain at 7 T** *Neuroimage* **107**:23–33 Google Scholar

Huo BX, Gao YR, Drew PJ (2015) **Quantitative separation of arterial and venous cerebral blood volume increases during voluntary locomotion** *Neuroimage* **105**:369–79 Google Scholar

Huo BX, Smith JB, Drew PJ (2014) **Neurovascular coupling and decoupling in the cortex during voluntary locomotion** *J Neurosci* **34**:10975–81 Google Scholar

Iadecola C, Smith EE, Anrather J, Gu C, Mishra A, et al. (2023) **The Neurovasculome: Key Roles in Brain Health and Cognitive Impairment: A Scientific Statement From the American Heart Association/American Stroke Association** *Stroke* Google Scholar

Jiang-Xie LF, Drieu A, Bhasiin K, Quintero D, Smirnov I, Kipnis J (2024) **Neuronal dynamics direct cerebrospinal fluid perfusion and brain clearance** *Nature* **627**:157–64 Google Scholar

Kara P, Friedlander MJ (1999) **Arginine analogs modify signal detection by neurons in the visual cortex** *J Neurosci* **19**:5528–48 Google Scholar

Karagiannis A, Gallopin T, David C, Battaglia D, Geoffroy H, et al. (2009) **Classification of NPY-expressing neocortical interneurons** *J Neurosci* **29**:3642–59 Google Scholar

Kawaguchi Y, Kubota Y (1997) **GABAergic cell subtypes and their synaptic connections in rat frontal cortex** *Cereb Cortex* **7**:476–86 Google Scholar

Kedarasetti RT, Drew PJ, Costanzo F (2022) **Arterial vasodilation drives convective fluid flow in the brain: a poroelastic model** *Fluids Barriers CNS* **19**:34 Google Scholar

Kilduff TS, Cauli B, Gerashchenko D (2011) **Activation of cortical interneurons during sleep: an anatomical link to homeostatic sleep regulation?** *Trends Neurosci* **34**:10–9 Google Scholar

Kjaerby C, Andersen M, Hauglund N, Untiet V, Dall C, et al. (2022) **Memory-enhancing properties of sleep depend on the oscillatory amplitude of norepinephrine** *Nat Neurosci* **25**:1059–70 Google Scholar

Knot HJ, Nelson MT (1998) **Regulation of arterial diameter and wall [Ca2+] in cerebral arteries of rat by membrane potential and intravascular pressure** *The Journal of Physiology* **508** Google Scholar

Kramer RS, Pearlstein RD (1979) **Cerebral cortical microfluorometry at isosbestic wavelengths for correction of vascular artifact** *Science* **205**:693–6 Google Scholar

Krawchuk MB, Ruff CF, Yang X, Ross SE, Vazquez AL (2020) **Optogenetic assessment of VIP, PV, SOM and NOS inhibitory neuron activity and cerebral blood flow regulation in mouse somato-sensory cortex** *J Cereb Blood Flow Metab* **40**:1427–40 Google Scholar

Kress BT, Iliff JJ, Xia M, Wang M, Wei HS, et al. (2014) **Impairment of paravascular clearance pathways in the aging brain** *Annals of Neurology* **76**:845–61 Google Scholar

Kubota Y, Shigematsu N, Karube F, Sekigawa A, Kato S, et al. (2011) **Selective coexpression of multiple chemical markers defines discrete populations of neocortical GABAergic neurons** *Cereb Cortex* **21**:1803–17 Google Scholar

Le Gac B, Tournissac M, Belzic E, Picaud S, Dusart I, et al. (2025) **Elevated pyramidal cell firing orchestrates arteriolar vasoconstriction through COX-2-derived prostaglandin E2 signaling** *eLife* :13 Google Scholar

Lee L, Boorman L, Glendenning E, Christmas C, Sharp P, et al. (2020) **Key Aspects of Neurovascular Control Mediated by Specific Populations of Inhibitory Cortical Interneurons** *Cereb Cortex* **30**:2452–64 Google Scholar

Li N, Chen S, Guo ZV, Chen H, Huo Y, et al. (2019) **Spatiotemporal constraints on optogenetic inactivation in cortical circuits** *eLife* :8 Google Scholar

Ma Y, Shaik MA, Kim SH, Kozberg MG, Thibodeaux DN, et al. (2016a) **Wide-field optical mapping of neural activity and brain haemodynamics: considerations and novel approaches** *Philos Trans R Soc Lond B Biol Sci* :371 Google Scholar

Ma Y, Shaik MA, Kozberg MG, Kim SH, Portes JP, et al. (2016b) **Resting-state hemodynamics are spatiotemporally coupled to synchronized and symmetric neural activity in excitatory neurons** *Proc Natl Acad Sci U S A* **113**:E8463–E71 Google Scholar

Mantyh PW, Allen CJ, Ghilardi JR, Rogers SD, Mantyh CR, et al. (1995) **Rapid endocytosis of a G protein-coupled receptor: substance P evoked internalization of its receptor in the rat striatum in vivo** *Proc Natl Acad Sci U S A* **92**:2622–6 Google Scholar

Martin JL, Sloviter RS (2001) **Focal inhibitory interneuron loss and principal cell hyperexcitability in the rat hippocampus after microinjection of a neurotoxic conjugate of saporin and a peptidase-resistant analog of Substance P** *The Journal of Comparative Neurology* **436**:127–52 Google Scholar

Mathis A, Mamidanna P, Cury KM, Abe T, Murthy VN, et al. (2018) **DeepLabCut: markerless pose estimation of user-defined body parts with deep learning** *Nat Neurosci* **21**:1281–89 Google Scholar

Matrongolo MJ, Ang PS, Wu J, Jain A, Thackray JK, et al. (2023) **Piezo1 agonist restores meningeal lymphatic vessels, drainage, and brain-CSF perfusion in craniosynostosis and aged mice** *Journal of Clinical Investigation* :134 Google Scholar

Matsumura S, Yamamoto K, Nakaya Y, O'Hashi K, Kaneko K, et al. (2021) **Presynaptic NK1 Receptor Activation by Substance P Suppresses EPSCs via Nitric Oxide Synthesis in the Rat Insular Cortex** *Neuroscience* **455**:151–64 Google Scholar

McKay LC, Feldman JL (2008) **Unilateral ablation of pre-Botzinger complex disrupts breathing during sleep but not wakefulness** *Am J Respir Crit Care Med* **178**:89–95 Google Scholar

Morairty SR, Dittrich L, Pasumarthi RK, Valladao D, Heiss JE, et al. (2013) **A role for cortical nNOS/NK1 neurons in coupling homeostatic sleep drive to EEG slow wave activity** *Proc Natl Acad Sci U S A* **110**:20272–7 Google Scholar

Osorio-Forero A, Cardis R, Vantomme G, Guillaume-Gentil A, Katsioudi G, et al. (2021) **Noradrenergic circuit control of non-REM sleep substates** *Curr Biol* **31**:5009–23 Google

Scholar

Paul A, Crow M, Raudales R, He M, Gillis J, Huang ZJ (2017) **Transcriptional Architecture of Synaptic Communication Delineates GABAergic Neuron Identity** *Cell* **171**:522–39 Google Scholar

Penny GR, Afsharpour S, Kitai ST (1986) **Substance P-immunoreactive neurons in the neocortex of the rat: A subset of the glutamic acid decarboxylase-immunoreactive neurons** *Neuroscience Letters* **65**:53–59 Google Scholar

Perrenoud Q, Geoffroy H, Gauthier B, Rancillac A, Alfonsi F, et al. (2012) **Characterization of Type I and Type II nNOS-Expressing Interneurons in the Barrel Cortex of Mouse** *Front Neural Circuits* **6**:36 Google Scholar

Pfeffer CK, Xue M, He M, Huang ZJ, Scanziani M (2013) **Inhibition of inhibition in visual cortex: the logic of connections between molecularly distinct interneurons** *Nat Neurosci* **16**:1068–76 Google Scholar

Phillips EA, Hasenstaub AR (2016) **Asymmetric effects of activating and inactivating cortical interneurons** *eLife* :5 Google Scholar

Pleil KE, Rinker JA, Lowery-Gionta EG, Mazzone CM, McCall NM, et al. (2015) **NPY signaling inhibits extended amygdala CRF neurons to suppress binge alcohol drinking** *Nat Neurosci* **18**:545–52 Google Scholar

Poplawsky AJ, Kim SG (2014) **Layer-dependent BOLD and CBV-weighted fMRI responses in the rat olfactory bulb** *Neuroimage* **91**:237–51 Google Scholar

Renden RB, Institoris A, Sharma K, Tran CHT (2024) **Modulatory effects of noradrenergic and serotonergic signaling pathway on neurovascular coupling** *Commun Biol* **7**:287 Google Scholar

Roth KA, Katz RJ (1979) **Stress, behavioral arousal, and open field activity--a reexamination of emotionality in the rat** *Neurosci Biobehav Rev* **3**:247–63 Google Scholar

Ruff CF, Juarez Anaya F, Dienel SJ, Rakymzhan A, Altamirano-Espinoza A, et al. (2024) **Long-range inhibitory neurons mediate cortical neurovascular coupling** *Cell Rep* **43**:113970 Google Scholar

Sahara S, Yanagawa Y, O'Leary DD, Stevens CF (2012) **The fraction of cortical GABAergic neurons is constant from near the start of cortical neurogenesis to adulthood** *J Neurosci* **32**:4755–61 Google Scholar

Schaeffer S, Iadecola C (2021) **Revisiting the neurovascular unit** *Nat Neurosci* **24**:1198–209 Google Scholar

Scherer-Singler U, Vincent SR, Kimura H, McGeer EG (1983) **Demonstration of a unique population of neurons with NADPH-diaphorase histochemistry** *J Neurosci Methods* **9**:229–34 Google Scholar

Schulz K, Sydekum E, Krueppel R, Engelbrecht CJ, Schlegel F, et al. (2012) **Simultaneous BOLD fMRI and fiber-optic calcium recording in rat neocortex** *Nature Methods* **9**:597–602 Google Scholar

Scott BB, Thiberge SY, Guo C, Tervo DGR, Brody CD, et al. (2018) **Imaging Cortical Dynamics in GCaMP Transgenic Rats with a Head-Mounted Widefield Macroscope** *Neuron* **100**:1045–58 Google Scholar

Seeger G, Hartig W, Rossner S, Schliebs R, Bruckner G, et al. (1997) **Electron microscopic evidence for microglial phagocytic activity and cholinergic cell death after administration of the immunotoxin 192IgG-saporin in rat** *Journal of neuroscience research* **48**:465–76 Google Scholar

Seibenhener ML, Wooten MC (2015) **Use of the Open Field Maze to measure locomotor and anxiety-like behavior in mice** *J Vis Exp* :e52434 Google Scholar

Shih AY, Mateo C, Drew PJ, Tsai PS, Kleinfeld D (2012) **A Polished and Reinforced Thinned-skull Window for Long-term Imaging of the Mouse Brain** *Journal of Visualized Experiments* Google Scholar

Sicher AR, Starnes WD, Griffith KR, Dao NC, Smith GC, et al. (2023) **Adolescent binge drinking leads to long-lasting changes in cortical microcircuits in mice** *Neuropharmacology* **234**:109561 Google Scholar

Sirotin YB, Das A. (2009) **Anticipatory haemodynamic signals in sensory cortex not predicted by local neuronal activity** *Nature* **457**:475–9 Google Scholar

Smith RJ, Anderson RI, Haun HL, Mulholland PJ, Griffin WC, et al. (2020) **Dynamic c-Fos changes in mouse brain during acute and protracted withdrawal from chronic intermittent ethanol exposure and relapse drinking** *Addict Biol* **25**:e12804 Google Scholar

Smith SL, Otis TS (2003) **Persistent changes in spontaneous firing of Purkinje neurons triggered by the nitric oxide signaling cascade** *J Neurosci* **23**:367–72 Google Scholar

Sohal VS, Zhang F, Yizhar O, Deisseroth K (2009) **Parvalbumin neurons and gamma rhythms enhance cortical circuit performance** *Nature* **459**:698–702 Google Scholar

Staiger JF, Petersen CCH (2021) **Neuronal Circuits in Barrel Cortex for Whisker Sensory Perception** *Physiol Rev* **101**:353–415 Google Scholar

Stringer C, Pachitariu M, Steinmetz N, Reddy CB, Carandini M, Harris KD (2019) **Spontaneous behaviors drive multidimensional, brainwide activity** *Science* **364**:255 Google Scholar

Tomioka R, Okamoto K, Furuta T, Fujiyama F, Iwasato T, et al. (2005) **Demonstration of long-range GABAergic connections distributed throughout the mouse neocortex** *Eur J Neurosci* **21**:1587–600 Google Scholar

Tomioka R, Rockland KS (2007) **Long-distance corticocortical GABAergic neurons in the adult monkey white and gray matter** *J Comp Neurol* **505**:526–38 Google Scholar

Tran CHT, Peringod G, Gordon GR (2018) **Astrocytes Integrate Behavioral State and Vascular Signals during Functional Hyperemia** *Neuron* **100**:1133–48 Google Scholar

Tricoire L, Vitalis T (2012) **Neuronal nitric oxide synthase expressing neurons: a journey from birth to neuronal circuits** *Front Neural Circuits* **6**:82 Google Scholar

Tu W, Cramer SR, Zhang N (2024) **Disparity in temporal and spatial relationships between resting-state electrophysiological and fMRI signals** *eLife* :13 Google Scholar

Turner KL, Gheres KW, Drew PJ (2023) **Relating Pupil Diameter and Blinking to Cortical Activity and Hemodynamics across Arousal States** *J Neurosci* **43**:949–64 Google Scholar

Turner KL, Gheres KW, Proctor EA, Drew PJ (2020) **Neurovascular coupling and bilateral connectivity during NREM and REM sleep** *eLife* :9 Google Scholar

Turrigiano GG (2008) **The self-tuning neuron: synaptic scaling of excitatory synapses** *Cell* **135**:422–35 Google Scholar

Uhlirova H, Kilic K, Tian P, Thunemann M, Desjardins M, et al. (2016) **Cell type specificity of neurovascular coupling in cerebral cortex** *eLife* :5 Google Scholar

van Veluw SJ, Hou SS, Calvo-Rodriguez M, Arbel-Ornath M, Snyder AC, et al. (2020) **Vasomotion as a Driving Force for Paravascular Clearance in the Awake Mouse Brain** *Neuron* **105**:549–61 Google Scholar

Vanlandewijck M, He L, Mae MA, Andrae J, Ando K, et al. (2018) **A molecular atlas of cell types and zonation in the brain vasculature** *Nature* **554**:475–80 Google Scholar

Vo TT, Im GH, Han K, Suh M, Drew PJ, Kim SG (2023) **Parvalbumin interneuron activity drives fast inhibition-induced vasoconstriction followed by slow substance P-mediated vasodilation** *Proc Natl Acad Sci U S A* **120**:e2220777120 Google Scholar

Vruwink M, Schmidt HH, Weinberg RJ, Burette A (2001) **Substance P and nitric oxide signaling in cerebral cortex: anatomical evidence for reciprocal signaling between two classes of interneurons** *J Comp Neurol* **441**:288–301 Google Scholar

Wang H, Germanson TP, Guyenet PG (2002) **Depressor and tachypneic responses to chemical stimulation of the ventral respiratory group are reduced by ablation of neurokinin-1 receptor-expressing neurons** *J Neurosci* **22**:3755–64 Google Scholar

Wiley RG, Lappi DA (1999) **Targeting neurokinin-1 receptor-expressing neurons with [Sar9,Met(O2)11 substance P-saporin** *Neurosci Lett* **277**:1–4 Google Scholar

Williams RH, Black SW, Thomas AM, Piquet J, Cauli B, Kilduff TS (2019) **Excitation of Cortical nNOS/NK1R Neurons by Hypocretin 1 is Independent of Sleep Homeostasis** *Cereb Cortex* **29**:1090–108 Google Scholar

Williams RH, Vazquez-DeRose J, Thomas AM, Piquet J, Cauli B, Kilduff TS (2018) **Cortical nNOS/NK1 Receptor Neurons are Regulated by Cholinergic Projections From the Basal Forebrain** *Cereb Cortex* **28**:1959–79 Google Scholar

Winder AT, Echagarruga C, Zhang Q, Drew PJ (2017) **Weak correlations between hemodynamic signals and ongoing neural activity during the resting state** *Nat Neurosci* **20**:1761–69 Google Scholar

Wölfle SE, Chaston DJ, Goto K, Sandow SL, Edwards FR, Hill CE (2011) **Non-linear relationship between hyperpolarisation and relaxation enables long distance propagation of**

vasodilatation *The Journal of physiology* **589**:2607–23 Google Scholar

Wright PW, Brier LM, Bauer AQ, Baxter GA, Kraft AW, et al. (2017) **Functional connectivity structure of cortical calcium dynamics in anesthetized and awake mice** *PLoS One* **12**:e0185759 Google Scholar

Wu YT, Bennett HC, Chon U, Vanselow DJ, Zhang Q, et al. (2022) **Quantitative relationship between cerebrovascular network and neuronal cell types in mice** *Cell Rep* **39**:110978 Google Scholar

Yan XX, Garey LJ (1997) **Morphological diversity of nitric oxide synthesising neurons in mammalian cerebral cortex** *J Hirnforsch* **38**:165–72 Google Scholar

Yan XX, Jen LS, Garey LJ (1996) **NADPH-diaphorase-positive neurons in primate cerebral cortex colocalize with GABA and calcium-binding proteins** *Cereb Cortex* **6**:524–9 Google Scholar

Zhang Q, Gheres KW, Drew PJ (2021) **Origins of 1/f-like tissue oxygenation fluctuations in the murine cortex** *PLoS Biol* **19**:e3001298 Google Scholar

Zhang Q, Haselden WD, Charpak S, Drew PJ (2023) **Could respiration-driven blood oxygen changes modulate neural activity?** *Pflugers Arch* **475**:37–48 Google Scholar

Zhang Q, Roche M, Gheres KW, Chaigneau E, Kedarasetti RT, et al. (2019) **Cerebral oxygenation during locomotion is modulated by respiration** *Nat Commun* **10**:5515 Google Scholar

Zhang Q, Turner KL, Gheres KW, Hossain MS, Drew PJ (2022) **Behavioral and physiological monitoring for awake neurovascular coupling experiments: a how-to guide** *Neurophotonics* **9**:021905 Google Scholar

Zhao J, Manza P, Wiers C, Song H, Zhuang P, et al. (2020) **Age-Related Decreases in Interhemispheric Resting-State Functional Connectivity and Their Relationship With Executive Function** *Frontiers in Aging Neuroscience* :12 Google Scholar

Zielinski MR, Atochin DN, McNally JM, McKenna JT, Huang PL, et al. (2019) **Somatostatin+/nNOS+ neurons are involved in delta electroencephalogram activity and cortical-dependent recognition memory** *Sleep* :42 Google Scholar

Author information

Kevin L Turner

Department of Engineering Science and Mechanics, The Pennsylvania State University, State College, United States, Center for Neural Engineering, The Pennsylvania State University, State College, United States, Department of Biomedical Engineering, The Pennsylvania State University, State College, United States, Penn State Neuroscience Institute, The Pennsylvania State University, State College, United States

Dakota F Brockway
Department of Biology, The Pennsylvania State University, State College, United States, Penn State Neuroscience Institute, The Pennsylvania State University, State College, United States

Md Shakhawat Hossain
Center for Neural Engineering, The Pennsylvania State University, State College, United States, Department of Biomedical Engineering, The Pennsylvania State University, State College, United States, Penn State Neuroscience Institute, The Pennsylvania State University, State College, United States

Keith R Griffith
Department of Biology, The Pennsylvania State University, State College, United States, Penn State Neuroscience Institute, The Pennsylvania State University, State College, United States

Denver I Greenawalt
Graduate Program in Molecular Cellular and Integrative Biosciences, The Pennsylvania State University, State College, United States, Penn State Neuroscience Institute, The Pennsylvania State University, State College, United States

Qingguang Zhang
Department of Engineering Science and Mechanics, The Pennsylvania State University, State College, United States, Center for Neural Engineering, The Pennsylvania State University, State College, United States, Penn State Neuroscience Institute, The Pennsylvania State University, State College, United States, Department of Physiology, Michigan State University, East Lansing, United States

Kyle W Gheres
Department of Engineering Science and Mechanics, The Pennsylvania State University, State College, United States, Center for Neural Engineering, The Pennsylvania State University, State College, United States, Penn State Neuroscience Institute, The Pennsylvania State University, State College, United States

Nicole A Crowley
Center for Neural Engineering, The Pennsylvania State University, State College, United States, Department of Biomedical Engineering, The Pennsylvania State University, State College, United States, Department of Biology, The Pennsylvania State University, State College, United States, Penn State Neuroscience Institute, The Pennsylvania State University, State College, United States
ORCID iD: 0000-0002-1142-7929

Patrick J Drew
Department of Engineering Science and Mechanics, The Pennsylvania State University, State College, United States, Center for Neural Engineering, The Pennsylvania State University, State College, United States, Department of Biomedical Engineering, The Pennsylvania State University, State College, United States, Department of Neurosurgery, The Pennsylvania State University, State College, United States, Penn State Neuroscience Institute, The Pennsylvania State University, State College, United States
ORCID iD: 0000-0002-7483-7378

For correspondence: pjd17@psu.edu

Editors

Reviewing Editor
Mark Nelson
University of Vermont, Burlington, United States of America

Senior Editor
Laura Colgin
University of Texas at Austin, Austin, United States of America

Reviewer #1 (Public review):

Turner et al. present an original approach to investigate the role of Type-1 nNOS interneurons in driving neuronal network activity and in controlling vascular network dynamics in awake head-fixed mice. Selective activation or suppression of Type-1 nNOS interneurons has previously been achieved using either chemogenetic, optogenetic or local pharmacology. Here, the authors took advantage of the fact that Type-1 nNOS interneurons are the only cortical cells that express the tachykinin receptor 1 to ablate them with a local injection of saporin conjugated to substance P (SP-SAP). SP-SAP causes cell death in 90 % of type1 nNOS interneurons without affecting microglia, astrocytes and neurons. The authors report that the ablation has no major effects on sleep or behavior. Refining the analysis by scoring neural and hemodynamic signals with electrode recordings, calcium signal imaging and wide field optical imaging, they observe that Type-1 nNOS interneuron ablation does not change the various phases of the sleep/wake cycle. However, it does reduce low-frequency neural activity, irrespective of the classification of arousal state. Analyzing neurovascular coupling using multiple approaches, they report small changes in resting-state neural-hemodynamic correlations across arousal states, primarily mediated by changes in neural activity. Finally, they show that nNOS type 1 interneurons play a role in controlling interhemispheric coherence and vasomotion.

In conclusion, these results are interesting, use state-of-the-art methods and are well supported by the data and their analysis. I have only a few comments on the stimulus-evoked haemodynamic responses that can be easily addressed:

Comments on revisions:

As I mentioned in my initial review, this study is important. In my opinion, it could be published as is. Nonetheless, I am still somewhat dissatisfied with the authors' responses to my earlier comments. I understand that the same animals were not used for both stimulation paradigms, which is unfortunate. Nonetheless, I would have appreciated it if the authors had provided a couple of experiments illustrating GCaMP7 signals during brief stimulation in their reply to the reviewers. I am still unconvinced by the authors' suggestion that the GCaMP7 signal would remain stable during removal of the vascular undershoot. Since the absence of the undershoot is notable, I anticipate that a significant part of the initial response to prolonged stimulation is influenced by processes that occur during the 0.1-second stimulation, processes that may involve a change in the bulk neuronal response.

In short, the data could support or refute the following statement: "Loss of type-I nNOS neurons drove minimal changes in the vasodilation elicited by brief stimulation..."

https://doi.org/10.7554/eLife.105649.2.sa2

Reviewer #2 (Public review):

Summary:

This important study by Turner et al., examines the functional role of a sparse but unique population of neurons in the cortex that express Nitric oxide synthase (Nos1). To do this, they pharmacolologically ablate these neurons in focal region of whisker related primary somatosensory (S1) cortex using a saponin-Substance P conjugate. Using widefield and 2-photon microscopy, as well as field recordings, they examine the impact of this cell specific lesion on blood flow dynamics and neuronal population activity. Within primary somatosensory cortex after Nos1 ablation, they find changes in neural activity patterns, decreased delta band power, reduced sensory evoked changes in blood flow (specifically eliminates the sustained blood flow change after stimulation) and decreased vasomotion.

Strengths:

This was a technically challenging study and the experiments were executed in an expert manner. The manuscript was well written and I appreciated the cartoon summary diagrams included in each figure. The analysis was rigorous and appropriate. Their discovery that Nos1 neurons can have significant effects on blood flow dynamics and neural activity is quite novel that should seed many follow up, mechanistic experiments to explain this phenomenon. The conclusions were justified by the convincing data presented.

Weaknesses:

I did not find any major flaws with the study. I originally noted some potential issues with the authors' characterization of the lesion and its extent, but that has been resolved in the revised manuscript.

Comments on revisions:

The authors have thoughtfully addressed the relatively minor concerns I had originally raised. Congratulations to the authors for producing this important paper.

https://doi.org/10.7554/eLife.105649.2.sa1

Author response:

The following is the authors' response to the original reviews.

> ***Reviewer #1 (Public review):***
>
> *Turner et al. present an original approach to investigate the role of Type-1 nNOS interneurons in driving neuronal network activity and in controlling vascular network dynamics in awake head-fixed mice. Selective activation or suppression of Type-1 nNOS interneurons has previously been achieved using either chemogenetic, optogenetic, or local pharmacology. Here, the authors took advantage of the fact that Type-1 nNOS interneurons are the only cortical cells that express the tachykinin receptor 1 to ablate them with a local injection of saporin conjugated to substance P (SP-SAP). SP-SAP causes cell death in 90 % of type1 nNOS interneurons without affecting microglia, astrocytes, and neurons. The authors report that the ablation has no major effects on sleep or behavior. Refining the analysis by scoring neural and hemodynamic signals with electrode recordings, calcium signal imaging, and wide-field optical imaging, the authors observe that Type-1 nNOS interneuron ablation does not change the various phases of the sleep/wake cycle. However, it does reduce low-frequency neural activity, irrespective of the classification of arousal state. Analyzing neurovascular coupling using*

> *multiple approaches, they report small changes in resting-state neural-hemodynamic correlations across arousal states, primarily mediated by changes in neural activity. Finally, they show that nNOS type 1 interneurons play a role in controlling interhemispheric coherence and vasomotion.*
>
> *In conclusion, these results are interesting, use state-of-the-art methods, and are well supported by the data and their analysis. I have only a few comments on the stimulus-evoked haemodynamic responses, and these can be easily addressed.*

We thank the reviewer for their positive comments on our work.

> ***Reviewer #2 (Public review):***
>
> *Summary:*
>
> *This important study by Turner et al. examines the functional role of a sparse but unique population of neurons in the cortex that express Nitric oxide synthase (Nos1). To do this, they pharmacologically ablate these neurons in the focal region of whisker-related primary somatosensory (S1) cortex using a saponin-substance P conjugate. Using widefield and 2photon microscopy, as well as field recordings, they examine the impact of this cell-specific lesion on blood flow dynamics and neuronal population activity. Locally within the S1 cortex, they find changes in neural activity paFerns, decreased delta band power, and reduced sensory-evoked changes in blood flow (specifically eliminating the sustained blood flow change amer stimulation). Surprisingly, given the tiny fraction of cortical neurons removed by the lesion, they also find far-reaching effects on neural activity paFerns and blood volume oscillations between the cerebral hemispheres.*
>
> *Strengths:*
>
> *This was a technically challenging study and the experiments were executed in an expert manner. The manuscript was well wriFen and I appreciated the cartoon summary diagrams included in each figure. The analysis was rigorous and appropriate. Their discovery that Nos1 neurons can have far-reaching effects on blood flow dynamics and neural activity is quite novel and surprising (to me at least) and should seed many follow-up, mechanistic experiments to explain this phenomenon. The conclusions were justified by the convincing data presented.*
>
> *Weaknesses:*
>
> *I did not find any major flaws in the study. I have noted some potential issues with the authors' characterization of the lesion and its extent. The authors may want to re-analyse some of their data to further strengthen their conclusions. Lastly, some methodological information was missing, which should be addressed.*

We thank the reviewer for their enthusiasm for our work.

> ***Reviewer #3 (Public review):***
>
> *The role of type-I nNOS neurons is not fully understood. The data presented in this paper addresses this gap through optical and electrophysiological recordings in adult mice (awake and asleep).*
>
> *This manuscript reports on a study on type-I nNOS neurons in the somatosensory cortex of adult mice, from 3 to 9 months of age. Most data were acquired using a combination of IOS and electrophysiological recordings in awake and asleep mice. Pharmacological ablation of the type-I nNOS populations of cells led to decreased coherence in gamma band coupling between lem and right hemispheres; decreased ultra-low frequency*

> *coupling between blood volume in each hemisphere; decreased (superficial) vascular responses to sustained sensory stimulus and abolishment of the post-stimulus CBV undershoot. While the findings shed new light on the role of type-I nNOS neurons, the etiology of the discrepancies between current observations and literature observations is not clear and many potential explanations are put forth in the discussion.*

We thank the reviewer for their comments.

> ***Reviewer #1 (Recommendations for the authors):***
>
> *(1) Figure 3, Type-1 nNOS interneuron ablation has complex effects on neural and vascular responses to brief (.1s) and prolonged (5s) whisker stimulation. During 0.1 s stimulation, ablation of type 1 nNOS cells does not affect the early HbT response but only reduces the undershoot. What is the pan-neuronal calcium response? Is the peak enhanced, as might be expected from the removal of inhibition? The authors need to show the GCaMP7 trace obtained during this short stimulation.*

Unfortunately, we did not perform brief stimulation experiments in GCaMP-expressing mice. As we did not see a clear difference in the amplitude of the stimulus-evoked response with our initial electrophysiology recordings (Fig. 3a), we suspected that an effect might be visible with longer duration stimuli and thus pivoted to a pulsed stimulation over the course of 5 seconds for the remaining cohorts. It would have been beneficial to interweave short-stimulus trials for a direct comparison between the complimentary experiments, but we did not do this.

> *During 5s stimulation, both the early and delayed calcium/vascular responses are reduced. Could the authors elaborate on this? Does this mean that increasing the duration of stimulation triggers one or more additional phenomena that are sensitive to the ablation of type 1 nNOS cells and mask what is triggered by the short stimulation? Are astrocytes involved? How do they interpret the early decrease in neuronal calcium?*

As our findings show that ablation reduces the calcium/vascular response more prominently during prolonged stimulation, we do suspect that this is due to additional NO-dependent mechanisms or downstream responses. NO is modulator of neural activity, generally increasing excitability (Kara and Friedlander 1999, Smith and Otis 2003), so any manipulation that changes NO levels will change (likely decrease) the excitability of the network, potentially resulting in a smaller hemodynamic response to sensory stimulation secondary to this decrease. While short stimuli engage rapid neurovascular coupling mechanisms, longer duration (>1s) stimulation could introduce additional regulatory elements, such as astrocytes, that operate on a slower time scale. On the right, we show a comparison of the control groups ploFed together from Fig. 3a and 3b with vertical bars aligned to the peak. During the 5s stimulation, the time-to-peak is roughly 830 milliseconds later than the 0.1s stimulation, meaning it's plausible that the signals don't separate until later. Our interpretation is that the NVC mechanisms responsible for brief stimulus-evoked change are either NO-independent or are compensated for in the SSP-SAP group by other means due to the chronic nature of the ablation.

We have added the following text to the Discussion (Line 368): "Loss of type-I nNOS neurons drove minimal changes in the vasodilation elicited by brief stimulation, but led to decreased vascular responses to sustained stimulation, suggesting that the early phase of neurovascular coupling is not mediated by these cells, consistent with the multiple known mechanisms for neurovascular coupling (AFwell et al 2010, Drew 2019, Hosford & Gourine 2019) acting through both neurons and astrocytes with multiple timescales (Le Gac et al 2025, Renden et al 2024, Schulz et al 2012, Tran et al 2018)."

Author response image 1.

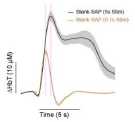

> *(2) In Figures 4d and e, it is unclear to me why the authors use brief stimulation to analyze the relationship between HbT and neuronal activity (gamma power) and prolonged stimulation for the relationship between HbT and GCaMP7 signal. Could they compare the curves with both types of stimulation?*

As discussed previously, we did not use the same stimulation parameters across cohorts. The mice with implanted electrodes received only brief stimulation, while those undergoing calcium imaging received longer duration stimulus.

> ***Reviewer #2 (Recommendations for the authors):***
>
> *(1) Results, how far-reaching is the cell-specific ablation? Would it be possible to estimate the volume of the cortex where Nos1 cells are depleted based on histology? Were there signs of neuronal injury more remotely, for example, beading of dendrites?*

We regularly see 1-2 mm in diameter of cell ablation within the somatosensory cortex of each animal, which is consistent with the spread of small molecules. Ribosome inactivating proteins like SAP are smaller than AAVs (~5 nm compared to ~25 nm in diameter) and thus diffuse slightly further. We observed no obvious indication of neuronal injury more remotely or in other brain regions, but we did not image or characterize dendritic beading, as this would require a sparse labeling of neurons to clearly see dendrites (NeuN only stains the cell body). Our histology shows no change in cell numbers.

We have added the following text to the Results (Line 124): “Immunofluorescent labeling in mice injected with Blank-SAP showed labeling of nNOS-positive neurons near the injection site. In contrast, mice injected with SP-SAP showed a clear loss in nNOS-labeling, with a typical spread of 1-2 mm from the injection site, though nNOS-positive neurons both subcortically and in the entirety of the contralateral hemisphere remaining intact.”

> *(2) For histological analysis of cell counts amer the lesion, more information is needed. How was the region of interest for counting cells determined (eg. 500um radius from needle/pipeFe tract?) and of what volume was analysed?*

The region of interest for both SSP-SAP and Blank SAP injections was a 1 mm diameter circle centered around the injection site and averaged across sections (typically 3-5 when available). In most animals, the SSP-SAP had a lateral spread greater than 500 microns and encompassed the entire depth of cortex (1-1.5 mm in SI, decreasing in the rostral to caudal direction). The counts within the 1 mm diameter ROI were averaged across sections and then converted into the cells per mm area as presented. Note the consistent decrease in type I nNOS cells seen across mice in Fig 1d, Fig S1b.

We have added the following text in the Materials & Methods (Line 507): “The region of interest for analysis of cell counts was determined based on the injection site for both SP-SAP and Blank SAP injections, with a 1 mm diameter circle centered around the injection site and averaged across 3-5 sections where available. In most animals, the SP-SAP had a lateral

spread greater than 500 microns and encompassed the entire depth of cortex (1-1.5 mm in SI)."

> *(3) Based on Supplementary Figure 1, it appears that the Saponin conjugate not only depletes Nos neurons but also may affect vascular (endothelial perhaps) Nos expression. Some quantification of this effect and its extent may be insighIul in terms of ascribing the effects of the lesion directly on neurons vs indirectly and perhaps more far-reaching via vascular/endothelial NOS.*

Thank you for this comment. While this is a possibility, while we have found that the high nNOS expression of type-I nnoos neurons makes NADPH diaphorase a good stain for detecting them, it is less useful for cell types that expres NOS at lower levels. We have found that the absolute intensity of NADPH diaphorase staining is somewhat variable from section to section. Variability in overall NADPH diaphorase intensity is likely due to several factors, such as duration of staining, thickness of the section, and differences in PFA concentration within the tissue and between animals. As NADPH diaphorase staining is highly sensitive to amount PFA exposure, any small differences in processing could affect the intensity, and slight differences in perfusion quality and processing could account. A second, perhaps larger issue could be due to differences in the number of arteries (which will express NOS at much higher levels than veins, and thus will appear darker) in the section. We did not stain for smooth muscle and so cannot differentiate arteries and veins. Any difference in vessel intensity could be due to random variations in the numbers of arteries/veins in the section. While we believe that this is a potentially interesting question, our histological experiments were not able to address it.

> *(4) The assessment for inflammation took place 1 month amer the lesion, but the imaging presumably occurred ~ 2 weeks amer the lesion. Note that it seemed somewhat ambiguous as to when approximately, the imaging, and electrophysiology experiments took place relative to the induction of the lesion. Presumably, some aspects of inflammation and disruption could have been missed, at the time when experiments were conducted, based on this disparity in assessment. The authors may want to raise this as a possible limitation.*

We apologize for our unclear description of the timeline. We began imaging experiments at least 4 weeks amer ablation, the same time frame as when we performed our histological assays.

We have added the following text to the Discussion (Line 379): "With imaging beginning four weeks amer ablation, there could be compensatory rewiring of local and/or network activity following type-I nNOS ablation, where other signaling pathways from the neurons to the vasculature become strengthened to compensate for the loss of vasodilatory signaling from the typeI nNOS neurons."

> *(5) Results Figure 2, please define "P or delta P/P". Also, for Figure 2c-f, what do the black vertical ticks represent?*

ΔP/P is the change in the gamma-band power relative to the resting-state baseline, and black tick marks indicate binarized periods of vibrissae motion ('whisking'). We have clarified this in Figure caption 2 (Line 174).

> *(6) Figure 3b-e, is there not an undershoot (eventually) amer 5s of stimulation that could be assessed?*

Previous work has shown that there is no undershoot in response to whisker stimulations of a few seconds (Drew, Shih, Kelinfeld, PNAS, 2011). The undershoot for brief stimuli happens within ~2.5 s of the onset/cessation of the brief stimulation, this is clearly lacking in the response to the 5s stim (Fig 3). The neurovascular coupling mechanisms recruited during the short stimulation are different than those recruited during the long stimulus, making a comparison of the undershoot between the two stimulation durations problematic.

> *For Figures 3e and 6 how was surface arteriole diameter or vessel tone measured? 2P imaging of fluorescent dextran in plasma? Please add the experimental details of 2P imaging to the methods. Including some 2P images in the figures couldn't hurt to help the reader understand how these data were generated.*

We have added details about our 2-photon imaging (FITC-dextran, full-width at half-maximum calculation for vessel diameter) as well as a trace and vessel image to Figure 2.

We have added the following text to the Materials & Methods (Line 477): “In two-photon experiments, mice were briefly anesthetized and retro-orbitally injected with 100 µL of 5% (weight/volume) fluorescein isothiocyanate–dextran (FITC) (FD150S, Sigma-Aldrich, St. Louis, MO) dissolved in sterile saline.”

We have added the following text to the Materials & Methods (Line 532): “A rectangular box was drawn around a straight, evenly-illuminated vessel segment and the pixel intensity was averaged along the long axis to calculate the vessel’s diameter from the full-width at half-maximum (hFps://github.com/DrewLab/Surface-Vessel-FWHM-Diameter; (Drew, Shih et al.

> *(7) Did the authors try stimulating other body parts (eg. limb) to estimate how specific the effects were, regionally? This is more of a curiosity question that the authors could comment on, I am not recommending new experiments.*

We did measure changes in [HbT] in the FL/HL representation of SI during locomotion (Line 205), which is known to increase neural activity in the somatosensory cortex (Huo, Smith and Drew, Journal of Neuroscience, 2014; Zhang et al., Nature Communications 2019). We observed a similar but not statistically significant trend of decreased [HbT] in SP-SAP compared to control. This may have been due to the sphere of influence of the ablation being centered on the vibrissae representation and not having fully encompassed the limb representation. We agree with the referee that it would be interesting to characterize these effects on other sensory regions as well as brain regions associated with tasks such as learning and behavior.

> *(8) Regarding vasomotion experiments, are there no other components of this waveform that could be quantified beyond just variance? Amplitude, frequency? Maybe these don't add much but would be nice to see actual traces of the diameter fluctuations. Further, where exactly were widefield-based measures of vasomotion derived from? From some seed pixel or ~1mm ROI in the center of the whisker barrel cortex? Please clarify.*

The reviewer’s point is well taken. We have added power spectra of the resting-state data which provides amplitude and frequency information. The integrated area under the curve of the power spectra is equal to the variance. Widefield-based measures of vasomotion were taken from the 1 mm ROI in the center of the whisker barrel cortex.

We have added the following text to the Materials & Methods (Line 560): “Variance during the resting-state for both Δ[HbT] and diameter signals (Fig. 7) was taken from resting-state events lasting ≥10 seconds in duration. Average Δ[HbT] from within the 1 mm ROI over the vibrissae

representation of SI during each arousal state was taken with respect to awake resting baseline events ≥10 seconds in duration."

> *(9) On page 13, the title seems like a bit strong. The data show a change in variance but that does not necessarily mean a change in absolute amplitude. Also, I did not see any reports of absolute vessel widths between groups from 2P experiments so any difference in the sampling of larger vs smaller arterioles could have affected the variance (ie. % changes could be much larger in smaller arterioles).*

We have updated the title of Figure 7 to specifically state power (which is equivalent to the variance) rather than amplitude (Line 331). We have also added absolute vessel widths to the Results (Line 340): "There was no difference in resting-state (baseline) diameter between the groups, with Blank-SAP having a diameter of 24.4 ± 7.5 μm and SP-SAP having a diameter of 23.0 ± 9.4 μm (Fest, p ti 0.61). "

> *(10) Big picture question. How could a manipulation that affects so few cells in 1 hemisphere (below 0.5% of total neurons in a region comprising 1-2% of the volume of one hemisphere) have such profound effects in both hemispheres? The authors suggest that some may have long-range interhemispheric projections, but that is presumably a fraction of the already small fraction of Nos1 neurons. Perhaps these neurons have specializing projections to subcortical brain nuclei (Nucleus Basilis, Raphe, Locus Coerulus, reticular thalamus, etc) that then project widely to exert this outsized effect? Has there not been a detailed anatomical characterization of their efferent projections to cortical and sub-cortical areas? This point could be raised in the discussion.*

We apologize for the lack of clarity of our work in this point. We would like to clarify that the only analysis showing a change in the unablated hemisphere being coherence/correlation analysis between the two hemispheres. Other metrics (LFP power and CBV power spectra) do not change in the hemisphere contralateral to the injections site, as we show in data added in two supplementary figures (Fig. S4 and 7). The coherence/correlation is a measure of the correlated dynamics in the two hemispheres. For this metric to change, there only needs to be a change in the dynamics of one hemisphere relative to another. If some aspects of the synchronization of neural and vascular dynamics across hemispheres are mediated by concurrent activation of type I nNOS neurons in both hemispheres, ablating them in one hemisphere will decrease synchrony. It is possible that type I nNOS neurons make some subcortical projections that were not reported in previous work (Tomioka 2005, Ruff 2024), but if these exist they are likely to be very small in number as they were not noted.

We have added the text in the Results (Line 228): "In contrast to the observed reductions in LFP in the ablated hemisphere, we noted no gross changes in the power spectra of neural LFP in the unablated hemisphere (Fig. S7) or power of the cerebral blood volume fluctuations in either hemisphere (Fig. S4)."

Line 335): "The variance in Δ[HbT] during rest, a measure of vasomotion amplitude, was significantly reduced following type-I nNOS ablation (Fig. 7a), dropping from 40.9 ± 3.4 μM^2 in the Blank-SAP group (N ti 24, 12M/12F) to 23.3 ± 2.3 μM^2 in the SP-SAP group (N ti 24, 11M/13F) (GLME p ti 6.9×10^{-5}) with no significant di[erence in the unablated hemisphere (Fig. S7)."

> ***Reviewer #3 (Recommendations for the authors):***
>
> *(1) The reporting would be greatly strengthened by following ARRIVE guidelines 2.0: hFps://arriveguidelines.org/: aFrition rates and source of aFrition, justification for the use of 119 (beyond just consistent with previous studies), etc.*

We performed a power analysis prior to our study aiming to detect a physiologically-relevant effect size of (Cohen's d) ti 1.3, or 1.3 standard deviations from the mean. Alpha and Power were set to the standard 0.05 and 0.80 respectively, requiring around 8 mice per group (SP-SAP, Blank, and for histology, naïve animals) for multiple independent groups (ephys, GCamp, histology). To potentially account for any aFrition due to failures in Type-I nNOS neuron ablation or other problems (such as electrode failure or window issues) we conservatively targeted a dozen mice for each group. Of mice that were imaged (1P/2P), two SP-SAP mice were removed from the dataset (24 SP-SAP remaining) post-histological analysis due to not showing ablation of nNOS neurons, an aFrition rate of approximately 8%.

We have added the following text to the Materials & Methods (Line 441): "Sample sizes are consistent with previous studies (Echagarruga et al 2020, Turner et al 2023, Turner et al 2020, Zhang et al 2021) and based on a power analysis requiring 8-10 mice per group (Cohen's d ti 1.3, α ti 0.05, (1 - β) ti 0.800). Experimenters were not blind to experimental conditions or data analysis except for histological experiments. Two SP-SAP mice were removed from the imaging datasets (24 SP-SAP remaining) due to not showing ablation of nNOS neurons during post-histological analysis, an aFrition rate of approximately 8%."

> *(2) Intro, line 38: Description of the importance of neurovascular coupling needs improvement. Coordinated haemodynamic activity is vital for maintaining neuronal health and the energy levels needed.*

We have added a sentence to the introduction (Line 41): "Neurovascular coupling plays a critical role in supporting neuronal function, as tightly coordinated hemodynamic activity is essential for meeting energy metabolism and maintaining brain health (Iadecola et al 2023, Schaeffer & Iadecola 2021)."

> *(3) Given the wide range of mice ages, how was the age accounted for/its effects examined?*

Previous work from our lab has shown that there is no change in hemodynamics responses in awake mice over a wide range of ages (2-18 months), so the age range we used (3 and 9 months of age) should not impact this.

We have added the following text in the Results (Line 437): "Previous work from our lab has shown that the vasodilation elicited by whisker stimulation is the same in 2–4-month-old mice as in 18-month-old mice (BenneF, Zhang et al. 2024). As the age range used here is spanned by this time interval, we would not expect any age-related differences."

> *(4) How was the susceptibility of low-frequency neuronal coupling signals to noise managed? How were the low-frequency bands results validated?*

We are not sure what the referee is asking here. Our electrophysiology recordings were made differentially using stereotrodes with tips separated by ~100μm, which provides excellent common-mode rejection to noise and a localized LFP signal. Previous publications from our lab (Winder et al., Nature Neuroscience 2017; Turner et al., eLife2020) and others (Tu, Cramer, Zhang, eLife 2024) have repeatedly show that there is a very weak correlation between the power in the low frequency bands and hemodynamic signals, so our results are consistent with this previous work.

> *(5) It would be helpful to demonstrate the selectivity of cell *death* (as opposed to survival) induced by SP-SAP injections via assessments using markers of cell death.*

We agree that this would be helpful complement to our histological studies that show loss of type-I nNOS neurons, but no loss of other cells and minimal inflammation with SP-saporin injections. However, we did not perform histology looking at cell death, only at surviving cells, given that we see no obvious inflammation or cells loss, which would be triggered by nonspecific cell death. Previous work has established that saporin is cytotoxic and specific only to cell that internalize the saporin. Internalization of saporin causes cell death via apoptosis (Bergamaschi, Perfe et al. 1996), and that the substance P receptor is internalized when the receptor is bound (Mantyh, Allen et al. 1995). Treatment of internalized saporin generates cellular debris that is phagocytosed by microglial, consistent with cell death (Seeger, Hartig et al. 1997). While it is possible that treatment of SP-saporin causes type 1 nNOS neurons to stop expressing nitric oxide synthase (which would make them disappear from our IHC staining), we think that this is unlikely given the literature shows internalized saporin is clearly cytotoxic.

We have added the following text to the Results (Line 131): “It is unlikely that the disappearance of type-I nNOS neurons is because they stopped expressing nNOS, as internalized saporin is cytotoxic. Exposure to SP-conjugated saporin causes rapid internalization of the SP receptor-ligand complex (Mantyh, Allen et al. 1995), and internalized saporin causes cell death via apoptosis (Bergamaschi, Perfe et al. 1996). In the brain, the resulting cellular debris from saporin administration is then cleared by microglia phagocytosis (Seeger, Hartig et al. 1997).”

> *(6) Was the decrease in inter-hemispheric correlation associated with any changes to the corpus callosum?*

We noted no gross changes to the structure of the corpus callosum in any of our histological reconstructions following SSPSAP administration, however, we did not specifically test for this. Again, as we note in our reply in reviewer 2, the decrease in interhemispheric synchronization does not imply that there are changes in the corpus callosum and could be mediated by the changes in neural activity in the hemisphere in which the Type-I nNOS neurons were ablated.

> *(7) How were automated cell counts validated?*

Criteria used for automated cell counts were validated with comparisons of manual counting as described in previous literature. We have added additional text describing the process in the Materials & Methods (Line 510): “For total cell counts, a region of interest (ROI) was delineated, and cells were automatically quantified under matched criteria for size, circularity and intensity. Image threshold was adjusted until absolute value percentages were between 1-10% of the histogram density. The function Analyze Par-cles was then used to estimate the number of particles with a size of 100-99999 pixels^2 and a circularity between 0.3 and 1.0 (Dao, Suresh Nair et al. 2020, Smith, Anderson et al. 2020, Sicher, Starnes et al. 2023). Immunoreactivity was quantified as mean fluorescence intensity of the ROI (Pleil, Rinker et al. 2015).”

> *(8) Given the weighting of the vascular IOS readout to the superficial tissue, it is important to qualify the extent of the hemodynamic contrast, ie the limitations of this readout.*

We have added the following text to the Discussion (Line 385): “Intrinsic optical signal readout is primarily weighted toward superficial tissue given the absorption and scaFering characteristics of the wavelengths used. While surface vessels are tightly coupled with neural activity, it is still a maFer of debate whether surface or intracortical vessels are a more

reliable indicator of ongoing activity (Goense et al 2012; Huber et al 2015; Poplawsky & Kim 2014)."

> *(9) Partial decreases observed through type-I iNOS neuronal ablation suggest other factors also play a role in regulating neural and vascular dynamics: data presented thus do *not* "indicate disruption of these neurons in diseases ranging from neurodegeneration to sleep disturbances," as currently stated. Please revise.*

We agree with the reviewer. We have changed the abstract sentence to read (Line 30): "This demonstrates that a small population of nNOS-positive neurons are indispensable for regulating both neural and vascular dynamics in the whole brain, raising the possibility that loss of these neurons could contribute to the development of neurodegenerative diseases and sleep disturbances."

https://doi.org/10.7554/eLife.105649.2.sa0